International Journal of Biological Macromolecules 362 (2026) 152143

Contents lists available at ScienceDirect

International Journal of Biological Macromolecules

journal homepage: www.elsevier.com/locate/ijbiomac

Marine antimicrobial peptide scyreprocin exhibits therapeutic potential against multidrug-resistant bacteria in wound and lung infections with low resistance

Xiaofei Wang [a], Xiao Hong [a], Huiyun Chen [a,b,c], Fangyi Chen [a,b,c], Ke-Jian Wang [a,b,c,*], Luxi Wang [d,**]

[a] State Key Laboratory of Marine Environmental Science, College of Ocean & Earth Sciences, Xiamen University, Xiamen, Fujian, China
[b] State-Province Joint Engineering Laboratory of Marine Bioproducts and Technology, College of Ocean & Earth Sciences, Xiamen University, Xiamen, Fujian, China
[c] Fujian Innovation Research Institute for Marine Biological Antimicrobial Peptide Industrial Technology, College of Ocean & Earth Sciences, Xiamen University, Xiamen, Fujian, China
[d] Department of Psychiatry and Department of Physiology, Sir Run Run Shaw Hospital School of Medicine, Zhejiang University, Hangzhou, Zhejiang, China

ARTICLE INFO

Keywords:
Multidrug-resistant bacteria
Antimicrobial peptide
Scyreprocin

ABSTRACT

Antibiotic resistance, driven by multidrug-resistant (MDR) pathogens, poses a major global health threat. Antimicrobial peptides (AMPs) have garnered significant attention as promising therapeutic agents for combating MDR bacteria. Here, we demonstrate the potent antimicrobial activity of scyreprocin against MDR strains, including *Staphylococcus aureus*, *Klebsiella pneumoniae*, *Acinetobacter baumannii*, and *Pseudomonas aeruginosa*. Notably, scyreprocin eradicated the tested strains without inducing drug resistance, inhibited biofilm formation, and eliminated persister cells. In terms of *in vivo* efficacy, scyreprocin displayed excellent activity against *S. aureus* and *K. pneumoniae* in a full-thickness wound infection model. Furthermore, administration of scyreprocin reduced bacterial burden in a *K. pneumoniae* lung infection model, thereby attenuating the pulmonary inflammatory response. Crucially, under cumulative administration of 25 mg/kg for 5 days, scyreprocin treatment *via* intravenous injection exerted no *in vivo* toxicity to mice. Mechanistic studies indicated that scyreprocin triggered membrane damage by causing rapid membrane permeability and leakage. Taken together, the marine-sourced scyreprocin demonstrates effective therapeutic potential for treating infections caused by drug-resistant pathogens.

1. Introduction

Antibiotic resistance constitutes a growing menace to human health, eliciting serious concerns within the global public health landscape [1,2]. Projections indicate that antibiotic-resistant infections are expected to account for 10 million deaths annually by 2050, a grim consequence attributed to the misuse and overuse of antibiotics [3]. The growing antibiotic resistance of pathogenic bacteria has exacerbated the issue of untreatable infections, especially with the rise of antibiotic-resistant "superbugs", such as the ESKAPE pathogens: *Enterococcus faecium*, *Staphylococcus aureus*, *Klebsiella pneumoniae*, *Acinetobacter baumannii*, *Pseudomonas aeruginosa* and *Enterobacter spp.*, which have become the primary causes of nosocomial infections [4,5]. Of notable concern is the widespread dissemination of plasmid-borne mobile antibiotic resistance genes [6,7], such as *mcr*-1 and NDM-1 [8,9], which confer resistance to colistin and carbapenems, respectively, crucially, these antibiotics are usually considered last-resort options for bacterial infections [10,11]. Additionally, the ability of ESKAPE pathogens to form biofilms exacerbates the resistance crisis, since the biofilm-encased bacteria significantly diminish the efficacy of conventional antibiotics [12,13]. Moreover, the presence of persister cells, a subpopulation of dormant bacterial cells with slow growth, contributes to antibiotic-tolerant chronic infections and recurrent infections [14,15]. Given the limited options within current antibiotic pipelines, there is an urgent

* Correspondence to: K-J. Wang, State Key Laboratory of Marine Environmental Science, College of Ocean & Earth Sciences, Xiamen University, Xiamen, Fujian, China.
** Corresponding author.
E-mail addresses: wkjian@xmu.edu.cn (K.-J. Wang), luxiwang@zju.edu.cn (L. Wang).

https://doi.org/10.1016/j.ijbiomac.2026.152143
Received 23 June 2025; Received in revised form 9 April 2026; Accepted 19 April 2026
Available online 20 April 2026

need for alternative therapeutic strategies that can effectively combat bacteria with acquired resistance while reducing the potential for further resistance development [16–18].

AMPs are essential components of the innate immune system, providing a robust defense against bacterial infections [19]. These short bioactive peptides, derived from a diverse range of organisms, are emerging as promising alternatives to classical antibiotics due to their potent antimicrobial activity, unique mechanisms of action, and low incidence of resistance [20–22]. AMPs primarily function by incorporating themselves into bacterial membranes, where the positively charged AMPs interact with negatively charged cellular membranes through electrostatic forces. Following bacterial targeting, based on structure-activity relationships, different AMPs usually adopting distinct structural scaffolds insert into lipid bilayers of bacterial membranes, resulting in membrane deformation and perturbation on bacteria. This interaction further permeabilizes and disrupts bacterial membranes, leading to cytoplasmic leakage and, ultimately, cell death [20,23,24]. Unlike conventional antibiotics, AMPs do not target a single bacterial component, which enhances their bactericidal effectiveness and reduces the likelihood of resistance development [20,25,26]. Additionally, AMPs can disrupt cellular processes by inhibiting the synthesis of cell wall, DNA, RNA and protein [27–30], further broadening their therapeutic potential.

Scyreprocin is a recently identified natural AMP that forms a functional complex with AMP SCY2 [31]. Previous studies have established its potent broad-spectrum antimicrobial activity against various microorganisms, including Gram-positive (*S. aureus*, *Bacillus subtilis*) and Gram-negative (*Escherichia coli*, *Pseudomonas stutzeri*) bacteria [32]. Simultaneously, scyreprocin exhibits effective antifungal activity with relatively low cytotoxicity toward mammalian cells. Beyond its antimicrobial properties, recent research has revealed that scyreprocin possesses anticancer activity, specifically targeting plasma membranes to induce apoptosis in NCI-H460 cancer cells. Notably, *in vivo* studies demonstrated a significant inhibition of NCI-H460 xenograft growth in nude mice [33], highlighting scyreprocin as a versatile, multi-functional therapeutic agent.

Despite these promising findings, the impact of scyreprocin on MDR pathogens remains to be further elucidated. In this study, we systematically explored the efficacy of scyreprocin against MDR bacteria. We performed a comprehensive evaluation of scyreprocin's stability under various experimental conditions, investigated its membrane permeation ability, and elucidated its mechanism of action. Furthermore, we examined its subcellular localization in bacterial cells, assessed the risk of resistance development, and determined its activity against biofilms and persister cells. To validate these *in vitro* findings, we employed distinct *in vivo* mouse infection models to determine whether scyreprocin retained its potent activity in a physiological context. Finally, we conducted rigorous toxicity evaluations both *in vitro* and *in vivo*. Collectively, our findings underscore the therapeutic potential of scyreprocin as a robust candidate for treating infections caused by MDR bacteria.

2. Materials and methods

2.1. Scyreprocin preparation and peptide synthesis

Scyreprocin was prepared following the previously described method from our laboratory [32]. Synthetic peptides (melittin, pexiganan, S-thanatin, and LL-37) were obtained *via* standard solid-phase peptide synthesis methods by GL Biochem (Shanghai, China). The purity and identity of each peptide were verified using high-performance liquid chromatography (HPLC) and mass spectrometry (MS).

2.2. Bacterial strains and chemical reagents

Standard bacterial strains, including *S. aureus* ATCC6538, *A. baumannii* ATCC19606, and *P. aeruginosa* ATCC9027, were purchased from the China General Microbiological Culture Collection Center (CGMCC). The clinical isolates listed in Table 1 were provided by the Second Affiliated Hospital of Fujian Medical University (Quanzhou, China). Both standard and clinical strains were cultured in Mueller-Hinton broth (HKM, China) at 37 °C. All antibiotics were purchased from Solarbio (Beijing, China), except for vancomycin, which was purchased from Sigma-Aldrich (Missouri, USA).

2.3. Antimicrobial susceptibility assay

2.3.1. Minimum inhibitory concentration (MIC) and minimum bactericidal concentration (MBC) assays

To investigate the efficacy of antimicrobial agents against ATCC and clinical strains, antimicrobial assays were performed using broth microdilution method recommended by the Clinical and Laboratory Standards Institute guidelines [34]. Briefly, bacteria grown to mid-exponential phase were diluted to 1×10^6 CFU/mL in MH broth, and 50 μL aliquots of bacterial suspensions were added to sterilized flat-bottom polypropylene microtiter plates (NEST, China). Subsequently, equivalent volumes of peptides or antibiotics were serially diluted across 96-well plates and incubated statically with the bacteria for 18–24 h at 37 °C. The MIC value was determined as the lowest concentration of peptide/antibiotic that prevented visible bacterial growth by visual inspection. The MBC was defined as the minimum concentration of AMPs capable of killing more than 99.99% of the initial inoculum. The tested concentration range was 3–48 μM. All MIC and MBC assays were performed in technical triplicates ($n = 3$) and repeated three independent times ($n = 3$).

2.3.2. Time-kill assay

Time-dependent killing assays were conducted on four MDR patho-

Table 1
Antimicrobial activity of AMPs against standard and MDR bacteria.

Bacteria	MICs (MBCs) of AMPs (μM)				
	Scyreprocin	Melittin	S-Thanatin	Pexiganan	LL-37
S. aureus ATCC6538	8 (8)	<3 (<3)	48 (>48)	6 (6)	12 (12)
MRSA QZ19132	8 (8)	6 (6)	48 (48)	6 (6)	12 (24)
MRSA QZ19133	8 (8)	<3 (<3)	48 (48)	6 (6)	12 (12)
MRSA QZ19134	4 (4)	<3 (<3)	>48 (>48)	12 (12)	12 (12)
K. pneumoniae QZ18106	4 (4)	6 (6)	<3 (3)	12 (12)	12 (12)
A. baumannii ATCC19606	8 (8)	<3 (<3)	6 (6)	6 (6)	6 (6)
A. baumannii QZ20143	>48 (>48)	<3 (<3)	6 (6)	6 (12)	6 (6)
A. baumannii QZ20144	4 (4)	12 (24)	6 (6)	12 (12)	12 (12)
A. baumannii QZ20145	8 (8)	6 (12)	6 (12)	6 (12)	12 (12)
P. aeruginosa ATCC9027	>48 (>48)	<3 (<3)	12 (12)	12 (12)	12 (12)
P. aeruginosa QZ18071	8 (16)	24 (24)	12 (12)	24 (24)	12 (12)
P. aeruginosa QZ18072	8 (8)	6 (6)	12 (12)	12 (12)	12 (24)
P. aeruginosa QZ18076	4 (4)	12 (12)	24 (24)	24 (24)	12 (12)
E. coli QZ20146	8 (16)	<3 (<3)	<3 (<3)	6 (6)	12 (12)
E. coli QZ20147	8 (8)	<3 (<3)	<3 (<3)	<3 (<3)	6 (6)
E. cloacae QZ18105	8 (8)	<3 (<3)	<3 (<3)	6 (6)	24 (24)

gens with minor modifications [35]. Briefly, bacteria were harvested at exponential phase and diluted to 1×10^6 CFU/mL in MH medium. Bacterial suspensions were then challenged with 1× MIC of scyreprocin or LL-37 at room temperature. At designated time points, aliquots were removed, diluted, and plated on nutrient agar plates (HKM, China). After overnight cultivation at 37 °C, colony-forming units (CFUs) were counted, and the killing efficacy was calculated using the following formula:

$$\%CFU = \text{recovered CFUs/initial CFUs} \times 100\%$$

The initial CFUs represented bacterial counts at 0 min, and recovered CFUs represented total viable counts at specific time intervals. Experiments were performed with three biologically independent samples ($n = 3$).

2.4. Thermal stability, ion-tolerance stability and cytotoxicity assays

Thermal and ion-tolerance assays were conducted to evaluate the stability of scyreprocin against four MDR bacteria [36]; pexiganan was used as a positive control. In brief, both scyreprocin and pexiganan were preincubated for 15 min at specified temperatures (4, 25, 50, 75, and 100 °C). Then, 50 μL of treated scyreprocin or pexiganan was incubated with an equivalent volume of bacteria (1×10^6 CFU/mL) overnight at 37 °C. Following incubation, MIC values were determined as described above. For the ion-tolerance assay, exponential-phase bacteria were diluted to 1×10^6 CFU/mL in MH medium containing 5 mM NaCl or $MgCl_2$, then 50 μL of suspensions were incubated with an equal volume of scyreprocin or pexiganan overnight at 37 °C.

Cell viability was evaluated using the MTS assay [37]. RAW 264.7, CHO-K1, HEK-293T, and HaCaT cells were seeded in 96-well plates (ThermoFisher, USA) at a density of 1×10^5 cells/mL. Cells were cultured in Dulbecco's Modified Eagle Medium (DMEM) supplemented with 10% fetal bovine serum and 1% penicillin-streptomycin for 12 h in a 5% CO_2 atmosphere at 37 °C. Subsequently, 10 μL aliquots of scyreprocin at a final concentration ranging from 2.5 μM to 20 μM were added to each well. Melittin (12 μM) and sterilized Milli-Q water served as positive and negative controls, respectively. After a 24-h exposure, the spent medium was removed and replaced with complete DMEM containing MTS solution (Promega, USA) according to the manufacturer's instructions. Plates were incubated in the dark at 37 °C with 5% CO_2 for an additional 2 h. Absorbance at 490 nm was measured using a Microplate Reader (Tecan, Switzerland). Cell viability was expressed as the percentage of cell growth relative to unexposed control cells under identical conditions. Assays were performed with three biologically independent samples ($n = 3$).

2.5. Scanning and transmission electron microscopy analysis

The surface morphology of MDR bacteria treated with scyreprocin was observed using scanning electron microscopy (SEM) [38]. Briefly, overnight bacterial cultures were diluted to 1×10^7 CFU/mL and incubated with scyreprocin at 1× MIC for 30 min at 37 °C. After incubation, samples were centrifuged (4000 ×*g*, 10 min) to obtain cell pellets. The samples were washed twice in 50 mM sodium phosphate buffer (NaPB) and fixed overnight with 2.5% glutaraldehyde at 4 °C. The following day, samples were gently rinsed three times with buffer and deposited on poly-lysine-coated slides for 30 min at 4 °C. Samples were dehydrated through a graded ethanol series (30%, 50%, 70%, 90%, and 95%) for 15 min each, followed by two 20-min washes in 100% ethanol. After dehydration, samples were dried in a Critical Point Dryer (Leica CPD300, Germany) and sputter-coated with gold (Jeol JFC-1600, Japan). SEM images were acquired using a Zeiss SUPRA 55 microscope (Zeiss, Germany).

Both morphological characteristics and intracellular alterations of bacterial cells following scyreprocin treatment were evaluated by transmission electron microscopy (TEM) [39]. Bacteria suspensions (1×10^7 CFU/mL) were exposed to scyreprocin (1× MIC) for 30 min at 37 °C. Cell pellets were washed twice and embedded in 2% low melting point agarose. Samples were fixed overnight with 2.5% glutaraldehyde at 4 °C. Post-fixation was performed with 1% osmium tetroxide for 2 h at room temperature, followed by three rinses in Milli-Q water (15 min each). Samples were dehydrated in a graded ethanol series (30%, 50%, 70%, 90%, 95%, and 100%; 15 min each), rinsed in acetone, and embedded in epoxy resin. Ultrathin sections (70 nm) were collected on 3-mm copper grids and stained with uranyl acetate and lead citrate. Images were captured using an HT7800 TEM (Hitachi, Japan).

2.6. Cell wall/membrane component binding assay

The binding affinity between scyreprocin and cellular surface components was evaluated based on a previously published method with minor modifications [32]. Lipopolysaccharide from *Klebsiella pneumoniae* (L4268, Sigma-Aldrich, USA), *Pseudomonas aeruginosa* (L9143, Sigma-Aldrich, USA), phosphatidylglycerol (L863491, Macklin, China), and cardiolipin (710333P, Sigma-Aldrich, USA) were diluted to 20 μg/mL in 1× ELISA coating buffer (Solarbio, China). 100 μL aliquots of solutions were transferred to white, flat-bottom 96-well plates and statically incubated overnight at 4 °C. Samples were washed three times with PBS, and adherent components were blocked with 5% (*w/v*) non-fat milk for 2 h at 37 °C. After removal of blocking solution, scyreprocin was serially diluted with final concentrations ranging from 0.0625 μM to 1 μM, and 100 μL aliquots were added into each well. After a 2-h incubation at 37 °C, plates were washed three times with PBS. A rabbit anti-scyreprocin primary antibody solution (1:1000) was added and incubated for 2 h at 37 °C. Following three PBS washes, an HRP-labeled goat anti-rabbit IgG secondary antibody (1:1000) was added and incubated for 2 h at 37 °C. Absorbance at 595 nm was measured using a Microplate Reader (Tecan, Switzerland), and affinity constants (K_D) were calculated using GraphPad Prism 10. Assays were performed in three biologically independent replicates ($n = 3$).

2.7. Membrane permeability assay

2.7.1. SYTOX green assay

Membrane permeabilization was assessed on the Gram-positive MRSA QZ19134 using a SYTOX Green nucleic acid dye (ThermoFisher, USA); peptide LL-37 and antibiotic vancomycin served as positive and negative controls, respectively [40]. Overnight bacterial cultures were diluted to 1×10^6 CFU/mL in NaPB. Bacterial suspensions (50 μL) were mixed with SYTOX Green (0.5 μM) in a black, opaque, flat-bottom 96-well plate. The mixtures were incubated at room temperature, and baseline fluorescence was recorded at 2-min intervals for 10 min. Subsequently, equal volumes of scyreprocin (1× MIC), LL-37 (1× MIC), vancomycin (4 × MIC), or assay buffer were added. Fluorescence intensity was monitored at 2-min intervals for an additional 30 min using a Microplate Reader with 485 nm excitation and 525 nm emission wavelengths. Curves were plotted using GraphPad Prism 10. Assays were conducted in three biologically independent replicates ($n = 3$).

2.7.2. NPN uptake assay

Outer membrane permeability was evaluated in Gram-negative *K. pneumoniae* QZ18106, *A. baumannii* QZ20144, and *P. aeruginosa* QZ18076 using a fluorescent probe 1-*N*-phenylnaphthylamine (NPN) (Sigma-Aldrich, USA) with minor modifications [41]. Bacteria grown overnight were resuspended in HEPES buffer (5 mM HEPES and 5 mM glucose, pH 7.4), then suspensions of bacteria (1×10^6 CFU/mL) were pre-mixed with NPN (10 μM), and the mixtures were incubated for 10 min at room temperature. Afterwards, 50 μL of probe-labeled bacteria were incubated with equivalent amounts of peptides in a black, opaque flat-bottom 96-well plate. 0.1% Triton X-100 (TX-100) was used as a positive control [42], and untreated cells served as a negative control. Fluorescence was recorded at 2-minute intervals for 30 min on an

Infinite M200 Microplate reader with the excitation/emission wavelength of 350/420 nm. Experiments were performed in three biologically independent samples ($n = 3$).

2.7.3. SYTO 9/PI assay

Inner-membrane integrity was assessed against Gram-negative *K. pneumoniae* QZ18106, *A. baumannii* QZ20144, and *P. aeruginosa* QZ18076 using a LIVE/DEAD *Bac*Light Bacterial Viability Kit (Invitrogen, USA) [41]. Bacterial suspensions (1×10^6 CFU/mL in NaPB) were incubated with scyreprocin (1× MIC) for 30 min in a black, clear-bottom 96-well plate (Cellvis, USA). The mixtures were gently rinsed twice in assay buffer and stained with SYTO 9 (1.67 μM) and PI (10 μM) for 15 min at room temperature in the dark. Fluorescent images were acquired using a confocal laser scanning microscope (Zeiss LSM 780, Germany) with a 100× oil immersion objective.

2.8. Membrane depolarization assay

Membrane depolarization following scyreprocin treatment was evaluated using a 3,3′-dipropylthiadicarbocyanine iodide [$DiSC_3(5)$] dye (Aladdin, China) [39]. Briefly, overnight cultures of bacteria were harvested and resuspended in HEPES buffer, then bacterial suspensions were diluted to 1×10^6 CFU/mL and mixed with 0.5 μM $DiSC_3(5)$ for 10 min at room temperature in the dark. Subsequently, 50 μL of the mixture was transferred to a black, opaque flat-bottom 96-well plate containing test peptides at a final concentration of 1× MIC. Fluorescence intensity was recorded using an Infinite M200 Microplate Reader (Ex = 620 nm, Em = 670 nm) at 2-min intervals for 30 min. LL-37 was used as a positive control, and assay buffer served as a negative control. Curves were plotted by GraphPad Prism 10. Assays were conducted in three biologically independent replicates ($n = 3$).

2.9. Reactive oxygen species (ROS) measurement

Intracellular ROS levels were measured using a 2′, 7′-Dichlorofluorescein diacetate (DCFH-DA) dye [43]. Bacterial suspensions (1×10^6 CFU/mL in PBS) were incubated with DCFH-DA (10 μM) for 10 min at room temperature. Labeled cells (50 μL) were then incubated with equivalent volumes of scyreprocin (1× MIC) or LL-37 (1× MIC) for another 30 min. Additionally, H_2O_2 (20 mM) was used as a positive control. ROS levels were immediately analyzed by flow cytometry (Beckman, USA) with the excitation/emission wavelength of 488/525 nm, and results were analyzed using CytExpert software.

2.10. Localization analysis by confocal microscopy

The subcellular localization of scyreprocin in MRSA QZ19134 was analyzed by confocal laser scanning microscopy [44]. In brief, an overnight culture of MRSA QZ19134 was washed twice and diluted to 1×10^7 CFU/mL, then 50 μL of bacterial suspensions were transferred in a black, clear-bottom 96-well plate. Later, the plate was supplemented with scyreprocin (1× MIC) for 30 min at room temperature. Subsequently, samples were fixed with 4% paraformaldehyde for 30 min and permeabilized for 10 min using 0.1% TX-100. Following incubation, samples were blocked in PBS with 5% BSA for 2 h at room temperature. Afterwards, the samples were incubated with rabbit anti-scyreprocin primary antibody (1:1000, diluted in PBS with 1% BSA) overnight at 4 °C. The following day, samples were incubated with goat anti-rabbit IgG secondary antibody (1:1000, diluted in PBS with 1% BSA) covalently labeled with red fluorescent dye Alexa Fluor 650 for 2 h in the dark. After three PBS washes, bacterial DNA was stained with DAPI for 15 min in the dark. Images were visualized using a Zeiss LSM 780 confocal microscope with a 100× oil immersion objective.

2.11. Subcellular localization via immunogold TEM

The subcellular localization of scyreprocin within Gram-negative bacteria was investigated using an immunogold labeling method as previously described [45]. In short, overnight bacterial cultures were harvested and resuspended in 0.1 M phosphate buffer (PB). Bacterial suspensions (1×10^7 CFU/mL) were incubated with scyreprocin at a concentration of 1× MIC for 30 min at room temperature. Following incubation, cells were pelleted (4000 ×*g*, 5 min), washed twice, and embedded in agar blocks. Samples were incubated on ice for 30 min and subsequently fixed in pre-cooled 4% paraformaldehyde containing 0.1% glutaraldehyde overnight at 4 °C. The following day, samples were dehydrated through a graded ethanol series (30%, 50%, 70%, 90%, 95%, and 100%) for 20 min each at 4 °C, followed by infiltration with LR White resin. Ultrathin sections (70 nm) were mounted on 3-mm copper grids and blocked with PB containing 1% BSA for 10 min at room temperature. Sections were then incubated with rabbit anti-scyreprocin primary antibody (1:100, diluted in PB) overnight at 4 °C. After washing three times with Milli-Q water, sections were incubated with goat anti-rabbit IgG secondary antibody (1:100, diluted in PB) labeled with 15-nm nanogold particles (EMS, USA) for 30 min at room temperature. Followed by three additional washes with Milli-Q water, sections were post-fixed with 2.5% glutaraldehyde solution, rinsed, and stained. Ultimately all images were acquired using an HT 7800 TEM. Experiments were conducted three independent times ($n = 3$).

2.12. Resistance development assay

The potential for resistance development against scyreprocin was evaluated following previously described methods [34,46]. Briefly, bacteria at mid-exponential phase were harvested and diluted to 1×10^6 CFU/mL. Bacterial suspensions (50 μL) were transferred to 96-well polystyrene microplates containing serial dilutions of scyreprocin or control antibiotics in triplicate. Plates were incubated statically overnight at 37 °C. MIC values determined on the first day were recorded as the initial baseline. For subsequent passages, bacterial cultures from wells containing sub-inhibitory concentrations (0.5× MIC) showing visible growth were diluted 1:1000 into fresh medium containing serial dilutions of antimicrobial agents. The MICs were defined as described above and repeated daily for 25, 60, and 180 days. Experiments were carried out in triplicates.

2.13. Prevention of biofilm formation

The biofilm inhibitory activity of scyreprocin against MDR bacteria was evaluated according to a previously described method [47]. In short, bacteria at mid-exponential phase were harvested and diluted to 1×10^6 CFU/mL. Bacterial suspensions (50 μL) were transferred to a 96-well plate containing varying concentrations (0.25×, 0.5×, and 1× MIC) of scyreprocin. Sterile Milli-Q water and LL-37 (1× MIC) were used as negative and positive controls, respectively. The cultures were incubated statically at 37 °C in a humidified atmosphere for 24 h. Following incubation, supernatants were aspirated to remove planktonic bacteria. The remaining biofilms were fixed with methanol for 15 min at room temperature and subsequently stained with 100 μL of 0.1% crystal violet solution (Sigma-Aldrich, USA) for an additional 15 min in the dark. Following three washes with PBS, stained biofilms were solubilized with 33% acetic acid. Absorbance at 595 nm was measured to quantify biofilm mass. Experiments were performed with three biologically independent samples ($n = 3$).

2.14. Anti-persister activity assay

The bactericidal activity of scyreprocin against persister cells was evaluated according to a previously described method with minor modifications [46]. Briefly, bacteria at mid-exponential phase were

harvested, and bacterial suspensions were diluted to 1×10^6 CFU/mL. Aliquots (100 μL) were seeded into 96-well plates and incubated at 37 °C in a humidified atmosphere. After a 24-hour incubation, planktonic bacteria were removed, and the adherent cultures were treated with 100 μL of MH containing ciprofloxacin, tigecycline, imipenem, and amikacin at a concentration of 100× MIC to isolate persister cells. Following an additional 24-hour exposure, planktonic bacteria were discarded, and adherent persisters were dislodged into 50 μL of PBS by sonication for 5 min. Subsequently, the samples were challenged with an equal volume of scyreprocin (1× MIC) or LL-37 (1× MIC). Sterile Milli-Q water served as a negative control. At the designated time points, aliquots of diluted bacterial suspensions were spread onto nutrient agar plates. Viable bacterial counts were determined by enumerating CFUs. Experiments were performed with three biologically independent samples ($n = 3$).

2.15. Antimicrobial activity in a RAW 264.7 co-culture model

The antimicrobial efficacy of scyreprocin against MDR bacteria in the presence of eukaryotic cells was evaluated using a coculture model based on a previously described method with minor modifications [48]. Briefly, RAW 264.7 cells (1×10^5 cells/mL) were seeded into a 48-well plate and cultured in DMEM supplemented with 10% FBS. Cells were incubated for 12 h to achieve a confluent monolayer. Later, supernatant was removed, and fresh complete DMEM containing 1×10^4 CFU of the respective MDR strains was added. Immediately thereafter, the co-cultures were treated with scyreprocin (4× MIC), pexiganan (4× MIC), or antibiotics (1× MIC). Cultures were incubated for 24 h in a humidified atmosphere with 5% CO_2 at 37 °C. Vehicle controls (treated with sterile Milli-Q water) and blank controls (medium only) were included. After incubation, cell morphology was visualized using an optical microscope (Leica, Germany). Subsequently, samples were serially diluted and plated on nutrient agar plates. Bacterial colonies were calculated by enumerating CFUs after overnight incubation at 37 °C. Experiments were performed with three biologically independent samples ($n = 3$).

2.16. In vivo full-thickness wound infection model

All animal experiments and husbandry procedures were conducted in strict accordance with protocols approved by the Institutional Animal Care and Use Committees of Xiamen University. All animal experiments were approved by the Animal Ethics Committee of the Xiamen University (accreditation number of the laboratory, XMULAC20230053). Sample sizes for each trial were specified in the corresponding figure legends.

The full-thickness wound infection model was established according to previously described method with minor modifications [43]. In brief, MRSA QZ19134 or *K. pneumoniae* QZ18106 at mid-exponential phase were harvested and diluted to 1×10^6 CFU/mL in saline. 6- to 8-week-old female BALB/c mice were purchased from Beijing Vital River Laboratory. Mice were anesthetized *via* intraperitoneal injection of tribromoethanol at a single dose of 250 mg/kg, and dorsal hair was removed. Full-thickness wounds were created on the back using a 5-mm-diameter biopsy punch. Later, wounds were inoculated with either MRSA QZ19134 (1×10^6 CFU/mL, 10 μL) or *K. pneumoniae* QZ18106 (1×10^6 CFU/mL, 10 μL). 30 min post-infection, mice were randomly divided into three groups ($n = 5$ per group) and treated as follows: scyreprocin (1 mg/mL), vancomycin/tigecycline (2 mg/mL, positive control), or saline (vehicle control). Administration was repeated four times at 12-hour intervals. On day 10, wound tissues were excised, weighed, and homogenized. Bacterial burden was determined by CFU counting and expressed as individual data points between groups.

2.17. In vivo lung infection model

K. pneumoniae-induced lung infection model was established based on previously described methods with minor modifications [39,49]. Briefly, bacteria were prepared as described above. 6- to 8-week-old female mice were anesthetized *via* intraperitoneal administration of tribromoethanol (250 mg/kg). Subsequently, anesthetized mice were infected with 50 μL of the *K. pneumoniae* QZ18106 bacterial suspension (1×10^6 CFU/mL) by intratracheal instillation. 30 min post-infection, mice were randomly divided into three cohorts ($n = 5$ per group) and received different treatments: scyreprocin (1 mg/mL), tigecycline (2 mg/mL, positive control), or saline (vehicle control). Both saline and scyreprocin groups received four additional doses at 12-hour intervals. In contrast, the tigecycline-treated group received only a single dose at 30 min post-infection. At 60 h post-infection, blood samples were collected and incubated statically at room temperature for 30 min. Serum was isolated by centrifugation and stored at −80 °C. The levels of interleukin 6 (IL-6) and tumor necrosis factor alpha (TNF-α) in serum were quantified using ELISA kits (Neobioscience, China) according to the manufacturer's instructions. Additionally, mice were sacrificed, and lung tissues were collected, weighed, and homogenized in sterile PBS. Serial dilutions of each suspension were plated on nutrient agar plates for the enumeration of bacterial burden. CFU per unit mass of lung tissue was quantified. Representative lung sections were collected for standard hematoxylin and eosin (H&E) stain procedures.

2.18. In vivo toxicity evaluation

In vivo safety profile of scyreprocin was evaluated following a previously described method with minor modifications [50]. Briefly, female BALB/c mice (6 to 8 weeks old) were purchased from Beijing Vital River Laboratory, and randomly divided into three groups ($n = 5$ per group). The scyreprocin-treated group received a daily intravenous injection of 5 mg/kg *via* tail vein for 5 consecutive days. The saline group (vehicle control) was administered daily for 5 days. The melittin-treated group (positive control) received a single dose of 5 mg/kg. Mice were monitored daily for survival and adverse effects. After normal feeding for 6 days, blood samples were collected *via* retro-orbital puncture prior to euthanasia. Serum was isolated and analyzed for biochemical indices, including alanine aminotransferase (ALT), aspartate aminotransferase (AST), urea nitrogen (BUN), creatinine (CRE), sodium (Na^+), and potassium (K^+). Subsequently, mice were euthanized, and major organs (heart, liver, spleen, kidney, and lung) were harvested for histological analysis *via* standard H&E staining.

2.19. Statistical analysis

All experiments were performed in triplicate and repeated at least three times unless otherwise noted in the corresponding figure legends. Data are represented as mean ± standard deviations (SD). Statistical analyses were performed using GraphPad Prism 10 software. For comparisons involving multiple groups, a one-way analysis of variance (ANOVA) was utilized. Appropriate *post hoc* tests (Dunnett's, Tukey's) were carried out to correct for multiple comparisons, with specific details provided in the respective figure legends. Comparisons between two groups were analyzed using an unpaired Student's *t*-test. A *p*-value of <0.05 was considered statistically significant. n.s. denoted no statistical significance.

3. Results

3.1. Scyreprocin exhibits potent antimicrobial activity against MDR bacteria

To evaluate the bactericidal potential of scyreprocin, we first tested its activity against a panel of standard and clinical bacterial strains. As shown in Table 1, scyreprocin displayed broad-spectrum antimicrobial activity against both Gram-positive and Gram-negative bacteria, with MIC values ranging from 2 μM to 8 μM. To further benchmark its

effectiveness, we selected four well-characterized AMPs including melittin, S-thanatin, pexiganan, and LL-37 for comparison. While these reference peptides exhibited bactericidal potency comparable to scyreprocin against most pathogens, scyreprocin notably demonstrated superior anti-MRSA activity compared to S-thanatin. Collectively, these results confirm that scyreprocin possesses potent antimicrobial efficacy against both standard and clinical MDR strains.

3.2. Scyreprocin exerts rapid bactericidal activity against MDR bacteria

To characterize the time-kill kinetics of scyreprocin against MDR bacteria, we selected four representative ESKAPE pathogens: MRSA QZ19134, *K. pneumoniae* QZ18106, *A. baumannii* QZ20144, and *P. aeruginosa* QZ18076. As shown in Fig. S1, at a concentration of 1× MIC, scyreprocin completely eradicated all four tested clinical strains within 120 min. In contrast, LL-37 required 180 min to achieve a comparable bactericidal effect. Notably, scyreprocin exhibited higher efficacy than LL-37 against MRSA QZ19134, *K. pneumoniae* QZ18106, and *A. baumannii* QZ20144. Collectively, these results highlight scyreprocin's rapid and potent bactericidal activity against MDR bacteria, underscoring its potential as a highly effective therapeutic agent.

3.3. Scyreprocin disrupts membrane morphology and alters membrane structure of MDR bacteria

To elucidate the underlying mechanism of scyreprocin against MDR bacteria, we examined bacterial surface morphology and internal ultrastructure using SEM and TEM. As shown in Fig. 1A–D, in the absence

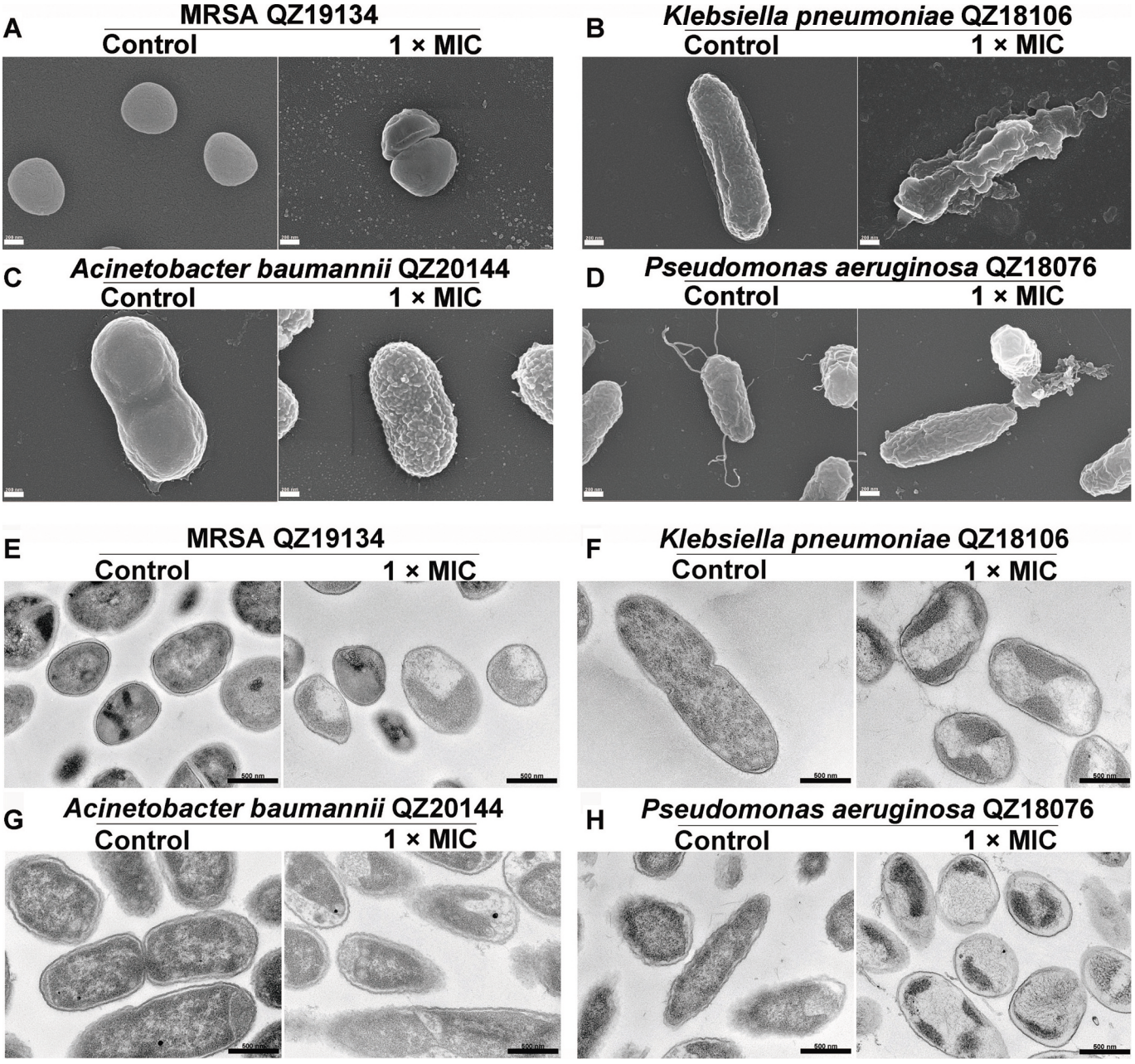

Fig. 1. Scyreprocin disrupts membrane morphology and ultrastructure of MDR bacteria.
(A–D) SEM images of MRSA QZ19134, *K. pneumoniae* QZ18106, *A. baumannii* QZ20144, and *P. aeruginosa* QZ18076 treated with scyreprocin (1× MIC) for 30 min. Control group was incubated in NaPB. Scale bars, 200 nm. **(E–H)** TEM images of MRSA QZ19134, *K. pneumoniae* QZ18106, *A. baumannii* QZ20144, and *P. aeruginosa* QZ18076 treated with scyreprocin (1× MIC) for 30 min. Control group was incubated in NaPB. Scale bars, 500 nm.

of scyreprocin, bacterial cells exhibited intact membranes with smooth surfaces. In contrast, scyreprocin treatment induced distinct morphological alterations in bacteria, characterized by significant membrane wrinkling and structural collapse compared to the controls. Furthermore, TEM analysis revealed that control cells showed clear, well-defined cell envelopes and dense intracellular contents (Fig. 1E–H). By contrast, scyreprocin treatment caused substantial permeabilization of bacterial membranes and decreased cytoplasmic density. Therefore, these results demonstrate that scyreprocin induces membrane damage in four MDR pathogens, elucidating its potent antibacterial mechanism.

3.4. Scyreprocin targets multiple components of bacterial membrane

The morphological damage observed by SEM and TEM strongly suggests that the primary mechanism of action of scyreprocin involves interacting with bacterial membrane. To validate this hypothesis, we evaluated the binding affinity of scyreprocin to key components of bacterial walls and membranes. As shown in Fig. S2A and B, scyreprocin exhibited high binding affinity for lipopolysaccharides, with K_D values of 5.8×10^{-4} μM and 3.2×10^{-3} μM, respectively. Additionally, scyreprocin displayed strong interactions with phospholipid components (Fig. S2C–D), binding to phosphatidylglycerol and cardiolipin with K_D values of 2.4×10^{-3} μM and 3.4×10^{-3} μM, respectively. These findings confirm that scyreprocin interacts with negatively charged components of bacterial membranes.

3.5. Scyreprocin enhances membrane permeability in MDR bacteria

A primary mechanism of action for many AMPs involves targeting and permeabilizing bacterial membranes [22]. To verify this, we assessed membrane integrity following scyreprocin treatment. As shown in Fig. 2A, scyreprocin (1× MIC) effectively permeated the cell membranes of MRSA QZ19134, as evidenced by a significant increase in intracellular SYTOX Green fluorescence. Additionally, scyreprocin exhibited superior permeabilizing efficacy compared to LL-37 (1× MIC) on MRSA QZ19134. Of note, 4× MIC of vancomycin failed to disrupt bacterial membrane integrity, a finding consistent with its mechanism of targeting cell wall synthesis rather than permeabilizing the bacterial membrane.

To further investigate the effect of scyreprocin on the complex envelope of MDR Gram-negative bacteria, we conducted leakage assays on *K. pneumoniae* QZ18106, *A. baumannii* QZ20144, and *P. aeruginosa* QZ18076 cells. The NPN uptake assay (Fig. 2B–D) revealed a significant increase in outer membrane permeability upon treatment with 1× MIC of scyreprocin, as indicated by enhanced NPN fluorescence intensity. Moreover, we evaluated inner membrane permeability using PI uptake assays (Figs. 2E–G and S3). Scyreprocin treatment resulted in marked increases in PI-uptake activity across all three pathogens, indicating substantial inner membrane disruption. Collectively, these findings demonstrate that scyreprocin induces significant damage to both outer and inner membranes of MDR Gram-negative bacteria. This dual disruption emphasizes scyreprocin's potent antibacterial mechanism against resistant strains.

3.6. Scyreprocin dissipates bacterial membrane potential of MDR bacteria

To further investigate the nature of membrane damage, we assessed the impact of scyreprocin on transmembrane potential using a voltage-sensitive fluorescence probe $DiSC_3(5)$. As shown in Fig. 2H–K, compared to untreated controls, scyreprocin (1× MIC) triggered a rapid and significant increase in fluorescence intensity across all tested MDR strains. This surge in fluorescence indicates that scyreprocin induces rapid membrane depolarization in MDR pathogens. Notably, this depolarizing effect was similar to that of the positive control, LL-37. These results confirm that scyreprocin effectively dissipates cell membrane potential, thereby collapsing the electrochemical gradient essential for bacterial survival.

3.7. Scyreprocin induces ROS accumulation in MDR bacteria

ROS generation is increasingly recognized as a universal mechanism underlying bacterial elimination induced by bactericidal antibiotics [51]. To evaluate whether oxidative stress contributes to the activity of AMPs, we measured intracellular ROS levels in four MDR strains following scyreprocin treatment. H_2O_2 (20 mM) solution served as the positive control. As shown in Fig. S4, at 1× MIC, scyreprocin treatment triggered a substantial accumulation of intracellular ROS across all tested MDR bacteria. This effect was comparable to that observed with the control peptide LL-37 (1× MIC). Moreover, the ROS-inducing capability of both scyreprocin and LL-37 was comparable to that of H_2O_2, a potent ROS inducer. These findings suggest that ROS accumulation is a crucial component of scyreprocin's bactericidal mechanism against MDR pathogens.

3.8. Scyreprocin localizes to both membrane and cytoplasm of MDR bacteria

To investigate the subcellular distribution of scyreprocin, we performed localization studies using confocal microscopy and immunogold TEM. As shown in Fig. S5A, immunofluorescence analysis revealed that scyreprocin specifically accumulated at the bacterial membranes of MRSA QZ19134, appearing as well-distributed signals compared to the control. To further determine the localization of scyreprocin in other Gram-negative bacteria, we employed immunogold labeling. As illustrated in Fig. S5B–D, no gold signals were observed in untreated control samples of *K. pneumoniae* QZ18106, *A. baumannii* QZ20144, and *P. aeruginosa* QZ18076. However, following scyreprocin treatment, gold nanoparticles were detected in bacterial cells. Notably, while a portion of these particles was localized to the cell membrane, the majority were dispersed throughout the cytoplasm. These observations suggest that scyreprocin penetrates intact bacterial membranes. Collectively, these data indicate that the molecular mechanism of scyreprocin involves both membrane targeting and cytoplasm penetration.

3.9. Scyreprocin exhibits a low propensity of resistance development

Unlike conventional antibiotics that often target specific intracellular machinery, AMPs primarily disrupt bacterial membranes, a mechanism associated with a significantly lower risk of resistance emergence [3,25,26]. To evaluate the potential for resistance development against scyreprocin, we performed serial passage assays on MRSA QZ19134, *K. pneumoniae* QZ18106, *A. baumannii* QZ20144, and *P. aeruginosa* QZ18076. As shown in Fig. 3A and Table S2, MRSA QZ19134 remained fully susceptible to scyreprocin over 60 days of consecutive passaging. The MIC values fluctuated only slightly (2-fold), ranging from 4 μM on day 1 to 8 μM on day 60. In sharp contrast, ciprofloxacin treatment triggered rapid resistance development in MRSA QZ19134, with the MIC increasing 128-fold (from 0.125 μg/mL to 16 μg/mL) [52,53].

Similarly, Fig. 3B showed that *K. pneumoniae* QZ18106 did not develop resistance to scyreprocin during an extended 180-day period of continuous exposure. MIC values remained stable between 4 μM and 8 μM. Conversely, under identical conditions, the strain developed high-level resistance (**Table S2**) to imipenem (MIC increased from 2 μg/mL to 256 μg/mL), meropenem (MIC increased from 4 μg/mL to 128 μg/mL), and tigecycline (MIC increased from 1 μg/mL to 128 μg/mL) [52,53]. Furthermore, scyreprocin exhibited no resistance induction against *A. baumannii* QZ20144 and *P. aeruginosa* QZ18076 under 25-day continuous cultivation (Fig. 3C-D**)**. MIC values shifted marginally from 4 μM to 8 μM for *A. baumannii* QZ20144 and remained constant at 4 μM for *P. aeruginosa* QZ18076, respectively. In contrast, as shown in Table S2, resistance was induced in *A. baumannii* QZ20144 by

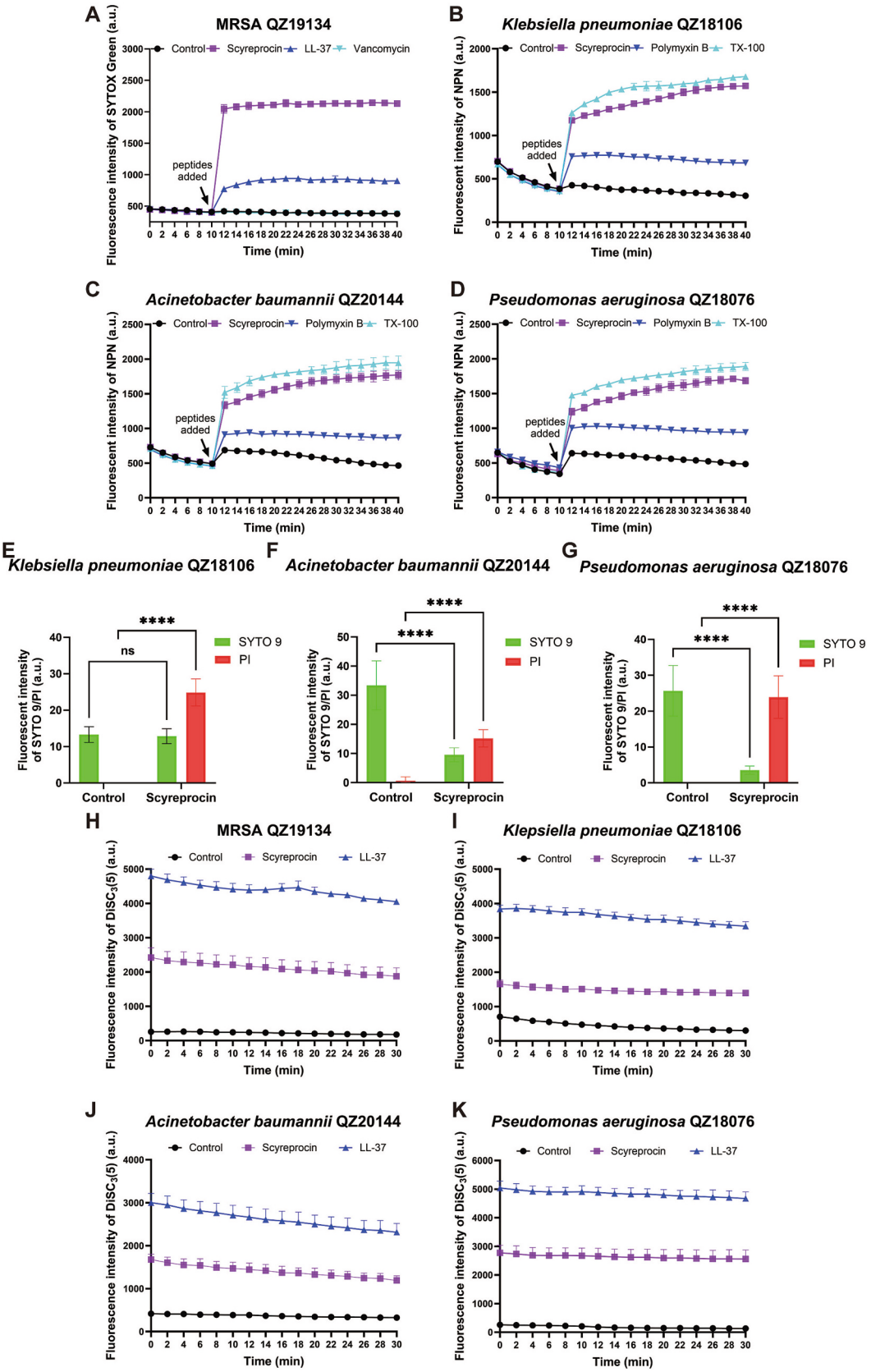

(caption on next page)

Fig. 2. Scyreprocin induces membrane permeabilization and depolarization in MDR bacteria.
(A) Membrane permeabilization of MRSA QZ19134 treated with scyreprocin (1× MIC), assessed by SYTOX Green fluorescence values. Vancomycin (4× MIC) and LL-37 (1× MIC) served as negative and positive controls, respectively. Data are presented as mean ± SD, $n = 3$ biologically independent samples. **(B–D)** Outer membrane permeability of *K. pneumoniae* QZ18106, *A. baumannii* QZ20144, and *P. aeruginosa* QZ18076 treated with scyreprocin (1× MIC), assessed by NPN fluorescence values. Polymyxin B (1× MIC) and 0.1% TX-100 were used as positive controls. Data are presented as mean ± SD, $n = 3$ biologically independent samples. **(E–G)** Inner membrane permeability of *K. pneumoniae* QZ18106, *A. baumannii* QZ20144, and *P. aeruginosa* QZ18076 treated with scyreprocin (1× MIC), detected by SYTO 9 and PI staining. Statistical analysis was performed using Student's *t*-test, ****$P < 0.0001$. $P > 0.05$ indicated no significance compared to the control (ns). $n = 3$ biologically independent replicates. **(H–K)** Membrane potential of MRSA QZ19134, *K. pneumoniae* QZ18106, *A. baumannii* QZ20144, and *P. aeruginosa* QZ18076 treated with scyreprocin (1× MIC), monitored by $DiSC_3(5)$ fluorescence values. LL-37 (1× MIC) and assay buffer served as positive and negative controls, respectively. Data are presented as mean ± SD, $n = 3$ biologically independent samples.

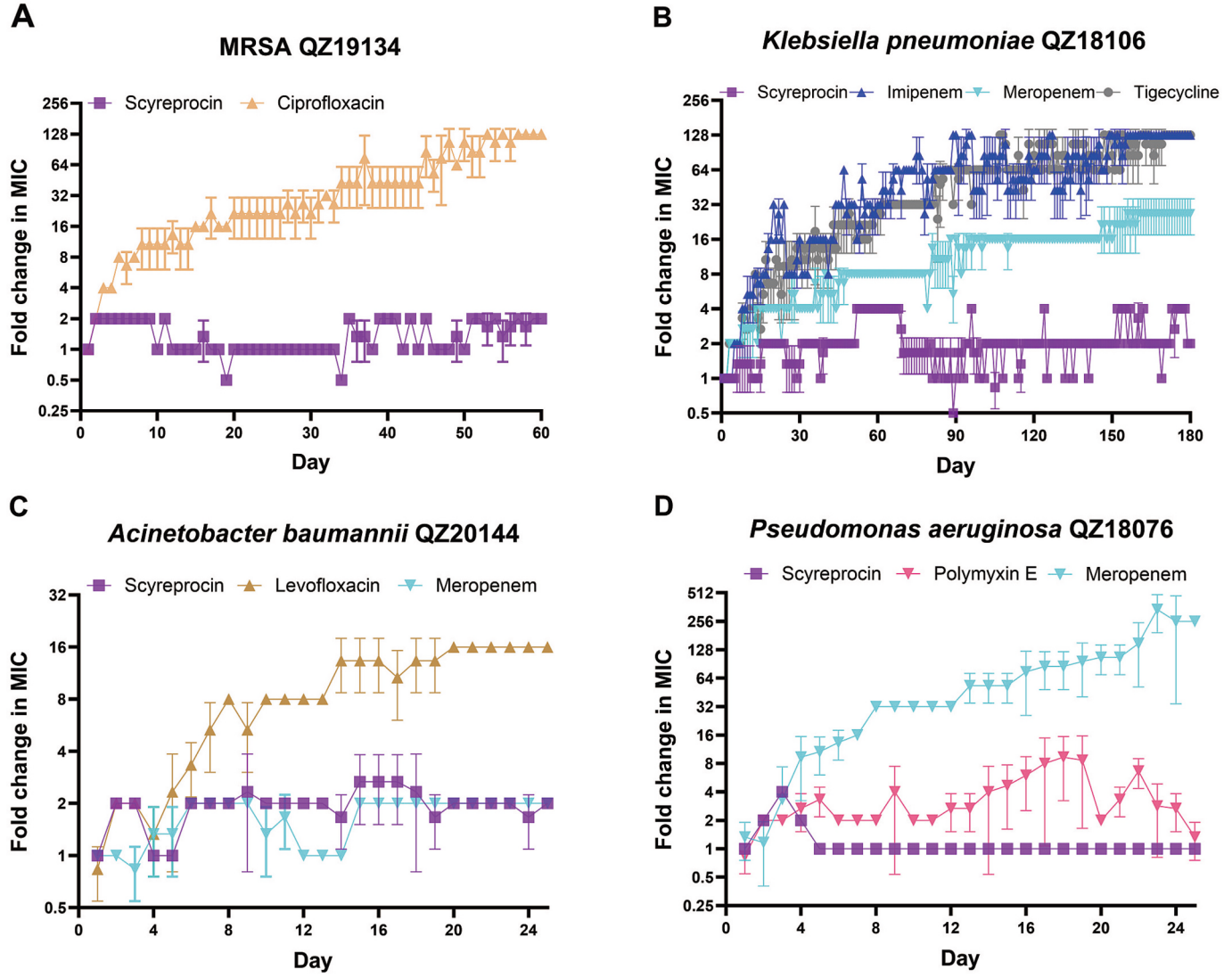

Fig. 3. Scyreprocin exhibits a low propensity for resistance development.
(A–D) Resistance acquisition curves for MRSA QZ19134, *K. pneumoniae* QZ18106, *A. baumannii* QZ20144, and *P. aeruginosa* QZ18076 following serial passage in the presence of scyreprocin or conventional antibiotics. The x-axis represented the experimental periods, the y-axis indicated fold changes in MIC relative to the initial MIC at day 1. Data are presented as mean ± SD, $n = 3$ biologically independent samples.

levofloxacin (MIC increased from 0.125 μg/mL to 2 μg/mL) and in *P. aeruginosa* QZ18076 by meropenem (MIC increased from 0.125 μg/mL to 32 μg/mL) [52,53]. In addition, meropenem (MIC increased from 0.125 μg/mL to 0.25 μg/mL) effectively killed *A. baumannii* QZ20144, and polymyxin E (MIC increased from 1 μg/mL to 2 μg/mL) maintained activity against *P. aeruginosa* QZ18076 [52,53]. Collectively, these data demonstrate that scyreprocin is a promising antimicrobial agent with a low propensity for inducing resistance in MDR bacteria.

3.10. Scyreprocin inhibits biofilm formation in MDR bacteria

Bacterial biofilms significantly exacerbate pathogenicity and play a key role in the development of antibiotic resistance [54]. To investigate the anti-biofilm potential of scyreprocin, we assessed its impact on biofilm formation across four MDR strains. As shown in Fig. S6, scyreprocin at 1× MIC effectively inhibited biofilm formation in MRSA QZ19134 and *A. baumannii* QZ20144. Notably, scyreprocin exhibited potent inhibitory effects against *K. pneumoniae* QZ18106 and

P. aeruginosa QZ18076 even at sub-inhibitory concentrations (0.25× MIC). Similarly, the control peptide LL-37 (1× MIC) inhibited biofilm formation across all four MDR pathogens. These findings suggest that scyreprocin functions as a potent anti-biofilm agent against MDR bacteria.

3.11. Scyreprocin efficiently eradicates persister cells

We further examined the bactericidal potency of scyreprocin against persister cells of MDR bacteria. As illustrated in Fig. 4A, persister cells of MRSA QZ19134 were generated by exposure to rifampicin (100× MIC) for 24 h. Subsequent treatment with scyreprocin (1× MIC) effectively killed ≥99.9% of these persisters within 4 h, achieving a median reduction of 1.2×10^8 CFU/mL. Similarly, as shown in Fig. 4B, scyreprocin (1× MIC) completely eradicated *K. pneumoniae* QZ18106 persisters (induced by 100× MIC of tigecycline), resulting in a median reduction of 9.8×10^7 CFU/mL. Furthermore, Fig. 4C demonstrated that scyreprocin (1× MIC) eliminated all *A. baumannii* QZ20144 persister cells (median reduction: 7.1×10^7 CFU/mL) under similar conditions. Likewise, more than 99.9% of *P. aeruginosa* QZ18076 persisters (induced by 100× MIC amikacin) were eradicated by scyreprocin (1× MIC) within 4 h, with a median reduction of 2.4×10^8 CFU/mL (Fig. 4D). The positive control, LL-37 (1× MIC), similarly achieved complete eradication across all four strains. Collectively, these results indicate that scyreprocin is a potent anti-persister agent capable of combating antibiotic-tolerant bacterial infections.

3.12. Scyreprocin exhibits high stability and low cytotoxicity

Stability and safety profiles are critical determinants for the translational potential of therapeutic peptides. We first evaluated the thermostability of scyreprocin against MRSA QZ19134, *K. pneumoniae* QZ18106, *A. baumannii* QZ20144, and *P. aeruginosa* QZ18076. As shown in Table S1, scyreprocin at 1× MIC retained full antimicrobial activity against the tested MDR strains even after exposure to elevated temperature, indicating that its efficacy is not compromised by thermal stress. In the ion-tolerance assay, scyreprocin (1× MIC) maintained its antimicrobial potency against above four MDR strains in the presence of 5 mM NaCl or $MgCl_2$, demonstrating that the presence of Na^+ and Mg^{2+} does not inhibit its activity. Additionally, the positive control AMP, pexiganan, exhibited comparable stability under thermal and ion-tolerance conditions.

Furthermore, we assessed the potential cytotoxicity of scyreprocin toward mammalian cells *in vitro*. As shown in Fig. S7, scyreprocin treatment at concentrations ranging from 2.5 to 20 μM did not significantly affect cellular viability of four mammalian cell lines (RAW 264.7, CHO-K1, HEK-293 T, and HaCaT) compared to the control group. In contrast, 12 μM of melittin remarkably reduced the viability of these cell lines. These findings indicate that scyreprocin exhibits minimal cytotoxicity toward mammalian cells at effective concentrations, highlighting its potential as a stable and safe therapeutic candidate.

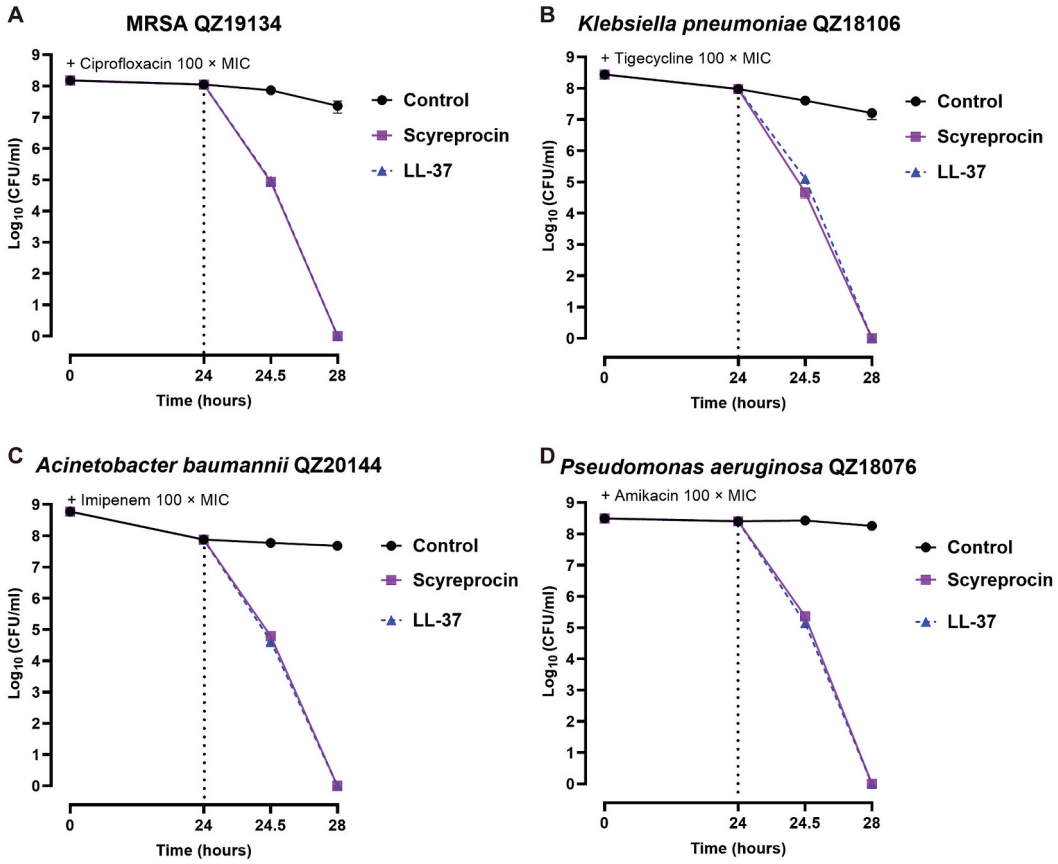

Fig. 4. Scyreprocin effectively eradicates persister cells of MDR bacteria.
Time-kill kinetics of persister cells treated with scyreprocin. Persister cells were generated by incubating pathogens for 24 h with 100× MIC of specific antibiotics: **(A)** MRSA QZ19134 (induced by ciprofloxacin), **(B)** *K. pneumoniae* QZ18106 (induced by tigecycline), **(C)** *A. baumannii* QZ20144 (induced by imipenem), and **(D)** *P. aeruginosa* QZ18076 (induced by amikacin). Subsequently, persisters were exposed to scyreprocin (1× MIC), LL-37 (1× MIC), or control buffer (no peptide) for an additional 4 h. Dotted lines indicated the time point of peptide addition. Bacterial viability was expressed as Log_{10} CFU/mL. Data are presented as mean ± SD, $n = 3$ biologically independent samples.

3.13. Scyreprocin eliminated extracellular MDR bacteria in RAW 264.7 co-culture model

To evaluate scyreprocin's efficacy against extracellular MDR bacteria in a physiological context, we employed an infection model of RAW 264.7 macrophage-bacteria co-culture. As depicted in Fig. 5A and B, after a 24-h co-culture, treatment with scyreprocin (4× MIC) effectively eradicated extracellular *K. pneumoniae* QZ18106, *A. baumannii* QZ20144, and *P. aeruginosa* QZ18076 bacteria. Bacterial loads in the supernatant were reduced to undetectable levels (0 CFU), demonstrating robust antibacterial activity against three MDR Gram-negative pathogens. Notably, morphological analysis in Fig. S8 revealed that while untreated RAW 264.7 cells suffered significant damage due to bacterial challenge, scyreprocin treatment effectively preserved cellular integrity.

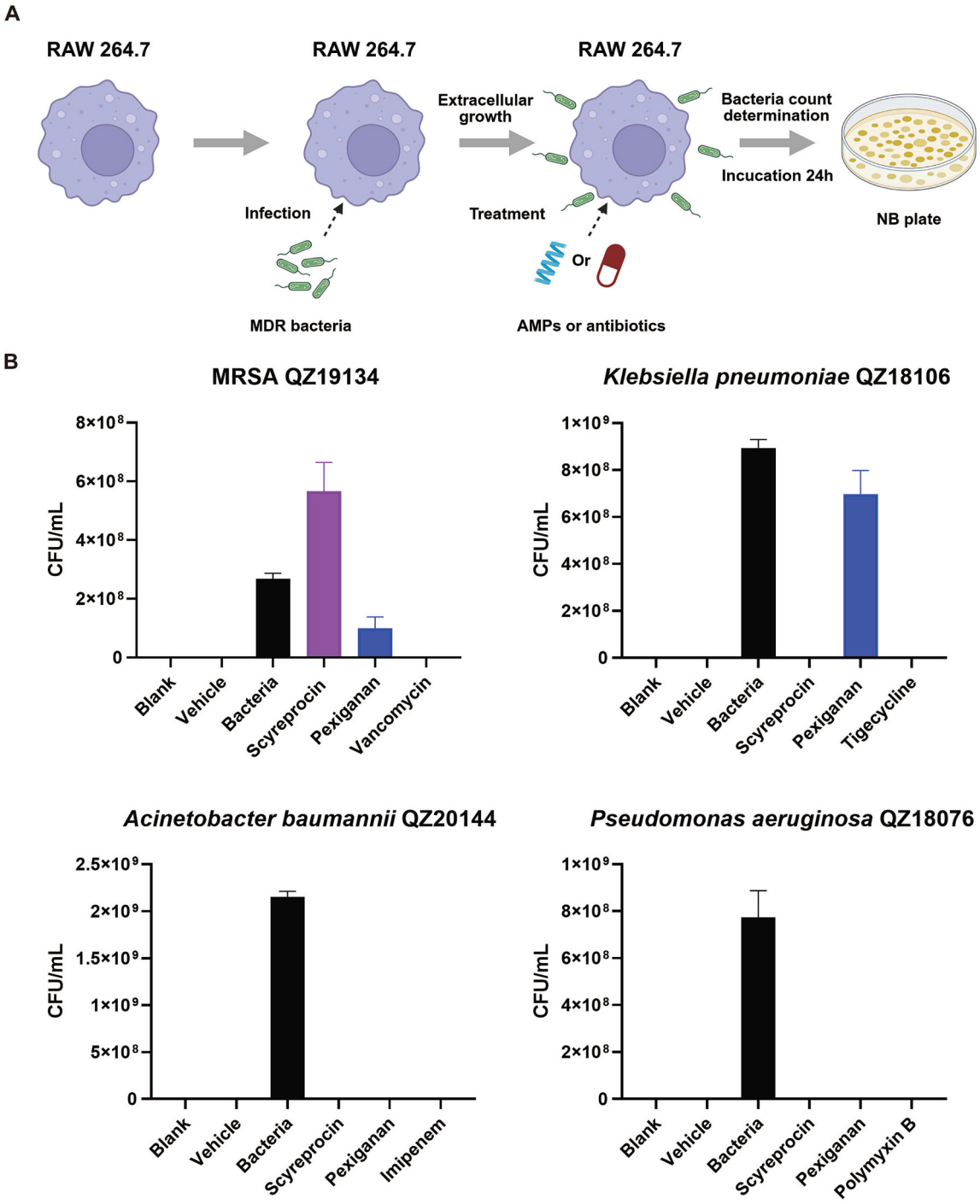

Fig. 5. Scyreprocin eliminates extracellular MDR bacteria in a macrophage co-culture model.
(A) Schematic illustration of establishment with RAW 264.7-bacterium co-culture model. RAW 264.7 cells (1×10^5 cells/mL, 200 μL) were seeded into 48-well plates and reached a confluent monolayer, bacterial suspensions (1×10^6 CFU/mL, 10 μL) of MRSA QZ19134, *K. pneumoniae* QZ18106, *A. baumannii* QZ20144, and *P. aeruginosa* QZ18076 were incubated with RAW 264.7 cells containing 4× MIC of scyreprocin, 4× MIC of pexiganan, or 1× MIC of antibiotics (vancomycin, tigecycline, imipenem, and polymyxin B), respectively. **(B)** Bacterial loads of MRSA QZ19134, *K. pneumoniae* QZ18106, *A. baumannii* QZ20144, and *P. aeruginosa* QZ18076 of extracellular supernatants of RAW 264.7 cells after distinct treatments at 24-hour incubation. Cells were incubated with or without sterile Milli-Q water, which served as vehicle control and blank control, respectively. Data are presented as mean ± SD, $n = 3$ biologically independent samples.

Moreover, as shown in Fig. S7, scyreprocin demonstrated no cytotoxic effects on RAW 264.7 cells at concentrations up to 20 μM. Collectively, these findings suggest that scyreprocin is a potent antibacterial agent capable of clearing extracellular infections while maintaining excellent compatibility with the host cells.

3.14. *In vivo efficacy of scyreprocin in MRSA and K. pneumoniae wound infections models*

Encouraged by the potent *in vitro* antimicrobial activity of scyreprocin, we further assessed its therapeutic potential *in vivo* using full-thickness wound models infected with MRSA QZ19134 or *K. pneumoniae* QZ18106. In the MRSA-infected wound model (Figs. 6A–B and S9A), multiple doses of scyreprocin resulted in an approximate 3-log reduction in bacterial burden compared to the saline group. This efficacy was on par with the therapeutic effects achieved with vancomycin. Similarly, in the *K. pneumoniae*-infected wound infection model (Figs. 6A–B and S9B), scyreprocin significantly reduced the bacterial load by approximately 3.1-log CFU compared to the saline group. This effect was comparable to that of tigecycline, demonstrating the potent *in vivo* efficacy of scyreprocin in treating wound infections.

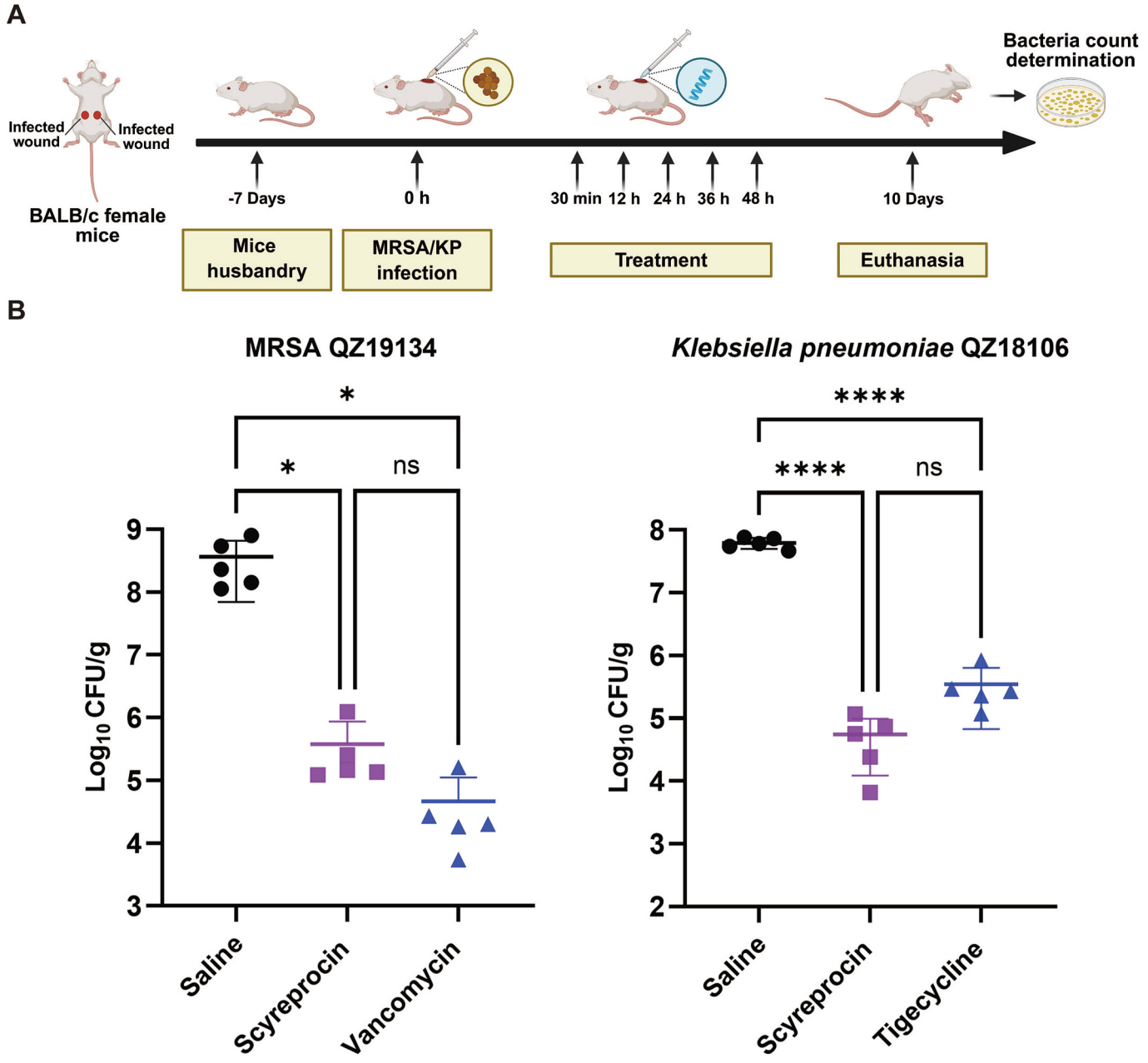

Fig. 6. Scyreprocin activity against MRSA QZ19134 and *K. pneumoniae* QZ18106 in a mouse wound infection model.
(A) Experimental design of the full-thickness skin wound infection model. Wounds were inoculated with 10 μL of a bacterial suspension (1×10^6 CFU/mL). 30-minute post infection, mice ($n = 5$ per group) received repeated topical treatment with saline, scyreprocin (1 mg/mL), or antibiotics (2 mg/mL). Abbreviations: MRSA, MRSA QZ19134; KP, *K. pneumoniae* QZ18106. **(B)** Quantification of bacterial burden in wound tissues. Left panel: Bacterial burden of the infected wounds after treatment with saline, scyreprocin (1 mg/mL), and vancomycin (2 mg/mL). Right panel: Bacterial burden of the infected wounds after treatment with saline, scyreprocin (1 mg/mL), and tigecycline (2 mg/mL). Data are presented as mean ± SD ($n = 5$ biologically independent animals). Statistical analysis was performed using Tukey's *post hoc* test, $^*P < 0.05$ and $^{****}P < 0.0001$. $P > 0.05$ indicated no significant difference between scyreprocin- and antibiotic-treated groups (ns).

3.15. Scyreprocin demonstrates therapeutic efficacy in a K. pneumoniae-induced pneumonia model

To further validate the therapeutic potential of scyreprocin, we evaluated its efficacy in a pneumonia model in mice infected with *K. pneumoniae* QZ18106. As shown in Fig. 7A–B, scyreprocin treatment significantly reduced pulmonary bacterial burden by approximately 2.1-log CFU relative to the saline-treated group. This efficacy was comparable to that of tigecycline, the current standard of care for *K. pneumoniae* infections. These data establish the potent therapeutic efficacy of scyreprocin in the lung infection model.

Furthermore, histopathological analysis of lung sections (Fig. 7C–D) revealed that scyreprocin treatment substantially alleviated lung lesions caused by bacterial infection, decreasing the infiltration of inflammatory cells and effectively mitigating pulmonary inflammation. Analysis of serum cytokine levels confirmed scyreprocin's systemic anti-inflammatory properties, as evidenced by a marked reduction in IL-6 and TNF-α levels. Collectively, these results highlight the potential antimicrobial and anti-inflammatory effects of scyreprocin *in vivo*, underscoring its therapeutic potential for treating lung infections caused by MDR bacteria.

3.16. Scyreprocin exhibits a favorable in vivo safety profile

While preceding studies established the therapeutic efficacy of scyreprocin, evaluating its *in vivo* safety profile is essential, particularly given that many conventional peptides and antibiotics are associated with severe nephrotoxicity [55,56] or hemolytic activity [57]. As shown in Fig. 8A and Fig. 8B, mice treated with scyreprocin at a cumulative dose of 25 mg/kg over 5 days maintained a 100% survival rate. However, the melittin-treated group experienced 100% mortality following a single dose of 5 mg/kg under identical experimental conditions. Additionally, no significant difference in body weight was observed between the scyreprocin-treated group and the saline control (Fig. 8C). Histological examination of major organs, including heart, liver, spleen, kidney, and lung, revealed normal morphology with no signs of pathological damage (Fig. S10). Importantly, serum biochemical analysis revealed that both ALT and AST levels remained within normal ranges, indicating that scyreprocin treatment did not induce acute hepatotoxicity. In addition, renal function profiles indicated no significant differences in serum BUN and CRE levels, suggesting a lack of nephrotoxicity. Electrolyte levels (specifically both K^+ and Na^+) remained normal, indicating the absence of electrolyte disturbance under scyreprocin treatment (Fig. 8D). Together, these data demonstrate that scyreprocin possesses a high safety margin, further supporting its

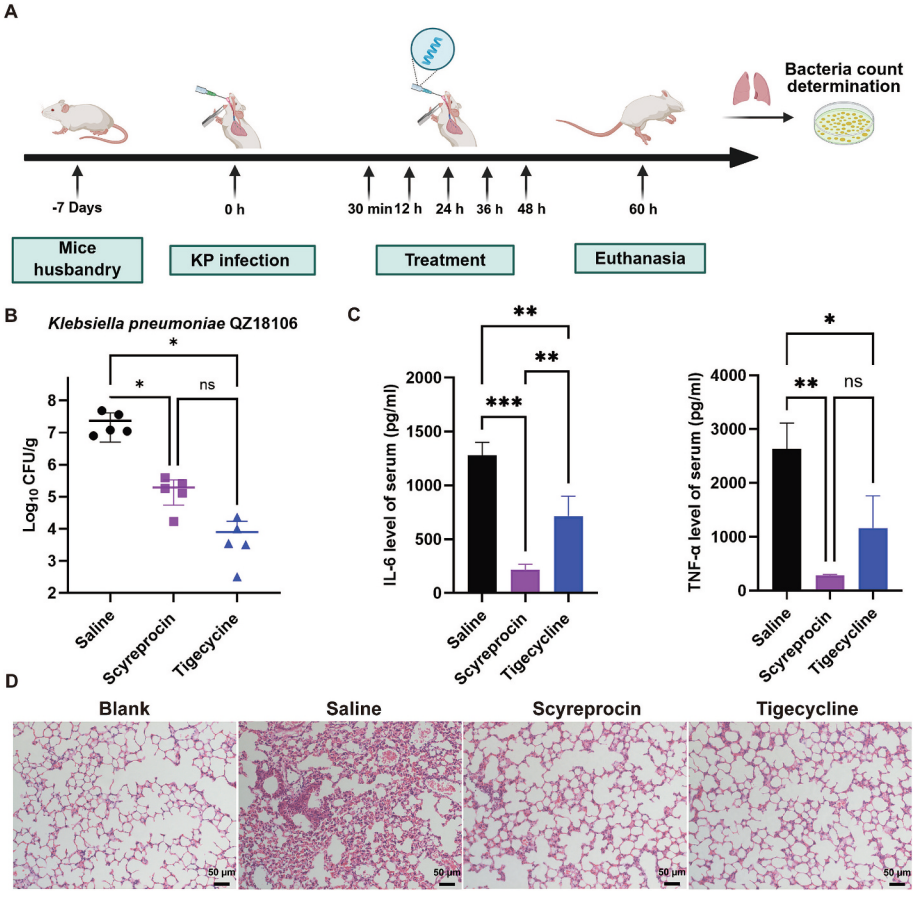

Fig. 7. Therapeutic efficacy of scyreprocin in a *K. pneumoniae* QZ18106-induced pneumonia model.
(A) Experimental design of the lung infection model. Mice were infected by intratracheal instillation of 50 μL of a *K. pneumoniae* QZ18106 suspension (1×10^6 CFU/mL). 30-minute post infection, mice ($n = 5$ per group) received repeated intratracheal administration with saline or scyreprocin (1 mg/mL). The tigecycline-treated group received a single dose at 30-minute post-infection. Abbreviations: KP, *K. pneumoniae* QZ18106. **(B)** Pulmonary bacterial burden after treatment with saline, scyreprocin (1 mg/mL), and tigecycline (2 mg/mL). Data are presented as mean ± SD ($n = 5$ biologically independent animals). Statistical analysis was performed using Tukey's *post hoc* test, $^*P < 0.05$. $P > 0.05$ indicated no significant difference between scyreprocin- and antibiotic-treated groups (ns). **(C)** Serum inflammatory cytokine levels of IL-6 and TNF-α from mice were examined by ELISA. Data are presented as mean ± SD ($n = 3$ biologically independent replicates). Statistical analysis was performed using Tukey's *post hoc* test, $^*P < 0.05$, $^{**}P < 0.01$, and $^{***}P < 0.001$. $P > 0.05$ indicated no significant difference (ns). **(D)** Representative lung sections after treatment with saline, scyreprocin, or tigecycline *via* H&E staining. The blank group represented the lungs from healthy, uninfected mice.

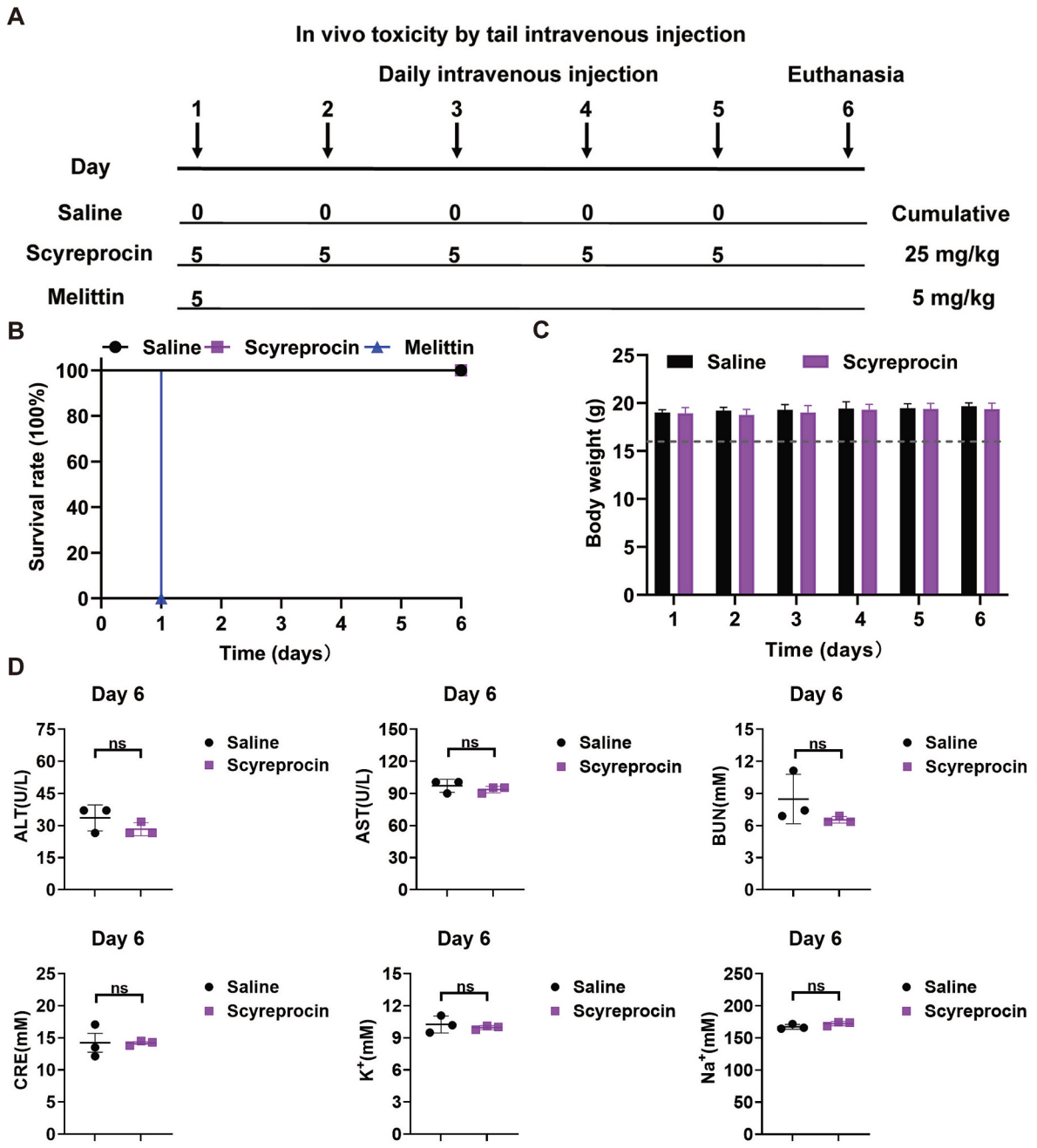

Fig. 8. *In vivo* safety evaluation of scyreprocin.
(A) Schematic illustration of the toxicity study design. BALB/c mice received intravenous injections of saline or scyreprocin (5 mg/kg) once daily for 5 consecutive days. As a positive control for toxicity, a separate group received a single dose of melittin (5 mg/kg). Survival rates **(B)** and body weight changes **(C)** were monitored during the 6-day experimental period ($n = 5$ biologically independent animals). **(D)** Serum biochemical indices (ALT, AST, BUN, CRE, K^+, and Na^+) on day 6 following a 5-day scyreprocin treatment (cumulative dose: 25 mg/kg). Data are presented as mean ± SD ($n = 3$ biologically independent replicates). Statistical analysis was performed using an unpaired Student's *t*-test. $P > 0.05$ indicated no significant difference compared to saline group (ns).

potential as a promising candidate for clinical application.

4. Discussion

Antibiotics have long served as a cornerstone of modern medicine, saving millions of lives over the past several decades as effective anti-infective drugs. However, the extensive use and misuse of these drugs have precipitated an alarming rise in antibiotic resistance [58,59], leading to frequent treatment failures against infections caused by MDR pathogens, particularly those of the ESKAPE family [4,5]. With the current antibiotic pipeline dwindling, there is an urgent need to identify novel therapeutic candidates that possess potent broad-spectrum antimicrobial activity and a reduced likelihood of inducing resistance. AMPs, as evolutionarily ancient components of the innate immune system, offer a rapid defense mechanism against pathogens by targeting and disrupting bacterial membranes [19,22,26]. Unlike disruption of specific biochemical pathways by conventional antibiotics, this membrane-targeting mechanism makes it difficult for bacteria to develop resistance [20,60]. Consequently, AMPs hold great promise as alternatives or supplements to traditional antibiotics, offering a potential solution to the escalating crisis of antibiotic resistance.

Several well-characterized AMPs, including melittin, pexiganan

[61], S-thanatin [62], and LL-37 [46], have demonstrated potent antimicrobial activity against MDR bacteria. Consistent with these findings, the newly identified marine-sourced AMP, scyreprocin, exhibited robust broad-spectrum antimicrobial efficacy against both Gram-positive and Gram-negative MDR strains in our study. Moreover, scyreprocin's profile mirrors that of SAAP-148, a promising pre-clinical candidate known for its potent efficacy in combating ESKAPE pathogens under physiological conditions [46]. Scyreprocin not only demonstrated excellent *in vitro* activity comparable to these reported AMPs but also exhibited high *in vivo* efficacy. These attributes contribute to fighting against MDR pathogens.

One of the most significant advantages of AMPs is their ability to evade resistance mechanisms. In our study, scyreprocin did not induce any resistance in MRSA QZ19134 even after a 60-day continuous exposure to sub-inhibitory peptide concentrations. Furthermore, it consistently maintained efficacy against difficult-to-treat Gram-negative pathogens, preventing the emergence of bacterial resistance (Fig. 3). In contrast, most traditional antibiotics rapidly induce resistance among ESKAPE pathogens during successive passages. The ability of scyreprocin to evade resistance development in MDR pathogens is likely due to its rapid, membrane-targeting mechanism [20,63,64], which physically disrupts the bacterial envelope rather than targeting specific mutable active sites. Another critical challenge in treating infections is bacterial biofilms, which significantly diminish antibiotic efficacy and represent a major unmet clinical need [54,65]. Consistent with previous findings on the AMP Spgillcin$_{177–189}$ from our lab [37], which significantly inhibited biofilm generation, scyreprocin demonstrated potent anti-biofilm activity by effectively preventing biofilm formation across four MDR strains. Moreover, persister cells, a subpopulation of highly antibiotic-tolerant, dormant, and slow-growing bacteria, represent a major challenge in treating chronic and recurrent infections [15,66]. Our results showed that scyreprocin efficiently eradicated over 99% of persister cells from four MDR strains within 4 h, highlighting its efficacy against this difficult-to-treat bacterial form (Fig. 4). While a previous study reported that the AMP LI14 exhibited bactericidal activity against persister cells [47], this peptide required a high concentration (32× MIC) to eliminate MRSA T144 and *E. coli* B2. Therefore, although LI14 showed a low toxicity profile, the substantial effective dosage limited its therapeutic advantage. In contrast, scyreprocin achieved complete eradication of MDR persisters at significantly lower concentrations (1× MIC), even when these bacteria survived high doses of conventional antibiotics. Consequently, scyreprocin displays potent activity against both antibiotic-resistance and antibiotic-tolerance phenotypes, positioning it as a promising candidate for clinical application.

To elucidate the mechanism of action of scyreprocin, we integrated microscopic observations with physicochemical analysis. SEM and TEM imaging revealed that scyreprocin physically disrupted the bacterial membrane of MDR pathogens. Given its cationic nature (net charge: +7) and high affinity for negatively charged components (Fig. S2), the initial step likely involves electrostatic interactions that facilitate the accumulation of peptide on the anionic bacterial surface [67]. In addition, scyreprocin possesses moderate hydrophobicity (27%) and adopts amphiphilic α–helical conformation, a structural feature critical for insertion into the hydrophobic core of bacterial lipid bilayers [68]. Subsequent permeation assays confirmed that this membrane-peptide interaction led to significant permeabilization of both Gram-positive and Gram-negative bacteria. Outer membrane of Gram-negative bacteria serves as a formidable barrier against many antibiotics. However, as shown in Fig. 2B–D, scyreprocin remarkably altered outer-membrane permeability of tested Gram-negative bacteria. Notably, scyreprocin exhibited superior permeabilizing potency compared to polymyxin B. The mechanism of polymyxin B primarily involves a high-affinity interaction with the lipid A component of lipopolysaccharide, and this step is likely shared by scyreprocin during its initial binding phase. At the same time, scyreprocin appears to induce more extensive membrane perturbation. This membrane disruption leads to a cascade of fatal events. We observed that the interaction not only altered membrane fluidity [69,70] but also dissipated transmembrane potential, thereby collapsing the electrochemical gradient essential for bacterial homeostasis. Furthermore, scyreprocin treatment triggered ROS-related accumulation levels, which correspondingly aggravated membrane damage and paralysed bacterial homoeostasis. In summary, scyreprocin manifested its sequential molecular mechanisms by binding anionic membrane components, inserting into the bacterial bilayer to alter membrane permeability, depolarizing membrane potential, and generating ROS, ultimately leading to membrane collapse and bacterial death.

Ensuring minimal toxicity is a prerequisite for the clinical translation of antimicrobial agents [44]. In our study, scyreprocin demonstrated negligible toxicity toward mammalian cells. Using a RAW 264.7 co-culture model, we found this peptide exhibited robust bactericidal activity against extracellular pathogens without inducing morphological damage to the host cells. Further *in vivo* assessments, involving multi-day treatment regimens to mimic clinical antibiotic therapy, revealed no signs of acute toxicity and positioned scyreprocin as a promising candidate. These findings align with reports on other biocompatible AMPs. For instance, the AMP horine exhibited no nephrotoxicity in mice after 1 week of intravenous injection, as evidenced by normal renal histology and biochemical indices [50]. Similarly, the AMP Ω76 displayed no toxic effects following repeated administration, as no significant differences in morphology by histopathological examination [44]. In contrast, the clinical development of many potent AMPs has been severely restricted by their high *in vivo* toxicity. A classic example is melittin, a strongly cytotoxic and lytic peptide. Our present results confirmed that melittin caused 100% mortality in mice even at low doses, consistent with the previous description [71]. To address such toxicity issues, researchers often employ modification strategies. For example, while the parental peptide poly-β-lysine caused 100% mortality in mice within 60 min, its derivative βLys$_{50}$HG$_{50}$, rationally designed to switch the mechanism from membrane disruption to membrane crossing, showed no *in vivo* toxicity for over 14 days [43]. Therefore, with potent antimicrobial activity and low toxicity profiles, scyreprocin holds promise as a safe and effective therapeutic agent in the fight against infection.

To further evaluate the therapeutic potential of scyreprocin, we employed full-thickness wound and lung infection models, which are widely utilized standards for evaluating the efficacy of preclinical candidates [49,72,73]. The clinical success of topical AMP pexiganan acetate in treating infected diabetic-foot ulcers serves as a precedent for this approach [74]. In the MRSA QZ19134 wound infection model, scyreprocin significantly reduced bacterial burden, mirroring the efficacy of a reported AMP βLys$_{50}$HG$_{50}$ against MRSA USA300 in skin wound tissue [43]. However, unlike βLys$_{50}$HG$_{50}$, scyreprocin exhibited potent activity against *K. pneumoniae* QZ18106 in the skin wound model. Therefore, scyreprocin was identified as a potent and broad-spectrum agent against ESKAPE pathogens, with its efficacy further validated in a pneumonia model. *K. pneumoniae* is a leading cause of both nosocomial and community-acquired pneumonia, and this specific bacterium-induced lung infection model is beneficial for exploring novel therapies [75]. Our results (Fig. 7) demonstrated that scyreprocin achieved therapeutic efficacy comparable to that of tigecycline, a last-resort antibiotic, in treating *K. pneumoniae* lung infections. This efficacy paralleled that of the AMP ZY4, which was reported to remarkably reduce *P. aeruginosa* burden in lung tissue [38]. Meanwhile, scyreprocin effectively modulated host immune responses under bacterial challenge, significantly reducing cytokine levels and alleviating inflammatory lesions in lungs. Collectively, our data demonstrate that scyreprocin possesses dual anti-infective and anti-inflammatory therapeutic potential, positioning it as a promising candidate against MDR bacterial infections.

Limiting factors still require attention. For example, drug resistance assay demonstrated that scyreprocin did not induce resistance development against ESKAPE pathogens. However, it is currently unclear whether scyreprocin consistently maintains its potent ability to kill

hypermutant bacteria responsible for rapid development of resistance, such as *E. coli* JW2703 ΔmutS::kan strain. Thus, further studies will analyze the evolution of resistance of *E. coli* JW2703 ΔmutS::kan bacteria following treatment with scyreprocin. *In vivo* study, scyreprocin exhibited broad-spectrum activity against both Gram-positive and Gram-negative bacteria in the full-thickness model, which serves as a standard model for acute skin infection in clinical settings. Nonetheless, chronic skin wounds represent a class of notorious diseases caused by difficult-to-treat bacterial infections, and we aim to advance the development of scyreprocin for treating diabetic chronic wound infections. Furthermore, scyreprocin showed no cumulative toxicity *in vivo via* intravenous administration. Next work will be focused on exploring a systemic regimen of scyreprocin in treating MDR bacterial infections, aiming to realize its clinical translation as soon as possible.

CRediT authorship contribution statement

Xiaofei Wang: Writing – original draft, Software, Methodology, Formal analysis. **Xiao Hong:** Software, Methodology. **Huiyun Chen:** Methodology. **Fangyi Chen:** Software, Methodology, Funding acquisition. **Ke-Jian Wang:** Writing – review & editing, Visualization, Validation, Supervision, Resources, Project administration, Investigation, Funding acquisition, Data curation, Conceptualization. **Luxi Wang:** Writing – review & editing, Writing – original draft, Visualization, Validation, Supervision, Project administration, Investigation, Funding acquisition, Formal analysis, Data curation, Conceptualization.

Funding

This work was supported by the National Natural Science Foundation of China (U1805233, 32200620); the Fujian Ocean and Fisheries Bureau (FJHY-YYKJ-2024-2-3); and the Xiamen Ocean Development Bureau (22CZP002HJ08).

Declaration of competing interest

Authors declare that they have no competing interests.

Acknowledgments

We thank the support from the Second Affiliated Hospital of Fujian Medical University, which provided MDR pathogens for scientific research. We thank Caiming Wu and Luming Yao of State Key Laboratory of Cellular Stress Biology, School of Life Sciences, Xiamen University for help with the electron microscopy observation. We also thank Marina Dukhinova of Zhejiang University for help with improving the quantity of writing.

Appendix A. Supplementary data

Supplementary data to this article can be found online at https://doi.org/10.1016/j.ijbiomac.2026.152143.

Data availability

Data will be made available on request.

References

[1] I.N. Okeke, M.E.A. de Kraker, T.P. Van Boeckel, C.K. Kumar, H. Schmitt, A.C. Gales, S. Bertagnolio, M. Sharland, R. Laxminarayan, The scope of the antimicrobial resistance challenge, Lancet 403 (2024) 2426–2438, https://doi.org/10.1016/S0140-6736(24)00876-6.
[2] S.J. Howard, S. Hopwood, S.C. Davies, Antimicrobial resistance: a global challenge, Sci. Transl. Med. 6 (2014) 236ed10, https://doi.org/10.1126/scitranslmed.3009315.
[3] C. Ghosh, P. Sarkar, R. Issa, J. Haldar, Alternatives to conventional antibiotics in the era of antimicrobial resistance, Trends Microbiol. 27 (2019) 323–338, https://doi.org/10.1016/j.tim.2018.12.010.
[4] W.R. Miller, C.A. Arias, ESKAPE pathogens: antimicrobial resistance, epidemiology, clinical impact and therapeutics, Nat. Rev. Microbiol. 22 (2024) 598–616, https://doi.org/10.1038/s41579-024-01054-w.
[5] D.M.P. De Oliveira, B.M. Forde, T.J. Kidd, P.N.A. Harris, M.A. Schembri, S. A. Beatson, D.L. Paterson, M.J. Walker, Antimicrobial resistance in ESKAPE pathogens, Clin. Microbiol. Rev. 33 (2020), https://doi.org/10.1128/CMR.00181-19 e00181-19.
[6] D.G.J. Larsson, C.F. Flach, Antibiotic resistance in the environment, Nat. Rev. Microbiol. 20 (2022) 257–269, https://doi.org/10.1038/s41579-021-00649-x.
[7] H. Zhou, J.F. Beltrán, I.L. Brito, Functions predict horizontal gene transfer and the emergence of antibiotic resistance, Sci. Adv. 7 (2021) eabj5056, https://doi.org/10.1126/sciadv.abj5056.
[8] Y.Y. Liu, Y. Wang, T.R. Walsh, L.X. Yi, R. Zhang, J. Spencer, Y. Doi, G. Tian, B. Dong, X. Huang, L.F. Yu, D. Gu, H. Ren, X. Chen, L. Lv, D. He, H. Zhou, Z. Liang, J.H. Liu, J. Shen, Emergence of plasmid-mediated colistin resistance mechanism MCR-1 in animals and human beings in China: a microbiological and molecular biological study, Lancet Infect. Dis. 16 (2016) 161–168, https://doi.org/10.1016/S1473-3099(15)00424-7.
[9] T.R. Walsh, J. Weeks, D.M. Livermore, M.A. Toleman, Dissemination of NDM-1 positive bacteria in the New Delhi environment and its implications for human health: an environmental point prevalence study, Lancet Infect. Dis. 11 (2011) 355–362, https://doi.org/10.1016/S1473-3099(11)70059-7.
[10] J.H. Liu, Y.Y. Liu, Y.B. Shen, J. Yang, T.R. Walsh, Y. Wang, J.Z. Shen, Plasmid-mediated colistin-resistance genes: *mcr*, Trends Microbiol. 32 (2024) 365–378, https://doi.org/10.1016/j.tim.2023.10.006.
[11] M. Acman, R.B. Wang, L. van Dorp, L.P. Shaw, Q. Wang, N. Luhmann, Y.Y. Yin, S. J. Sun, H.B. Chen, H. Wang, F. Balloux, Role of mobile genetic elements in the global dissemination of the carbapenem resistance gene, Nat. Commun. 13 (2022) 1131, https://doi.org/10.1038/s41467-022-28819-2.
[12] I. Olsen, Biofilm-specific antibiotic tolerance and resistance, Eur. J. Clin. Microbiol. Infect. Dis. 34 (2015) 877–886, https://doi.org/10.1007/s10096-015-2323-z.
[13] D. Sharma, L. Misba, A.U. Khan, Antibiotics versus biofilm: an emerging battleground in microbial communities, Antimicrob. Resist. Infect. Control 8 (2019) 76, https://doi.org/10.1186/s13756-019-0533-3.
[14] R.A. Fisher, B. Gollan, S. Helaine, Persistent bacterial infections and persister cells, Nat. Rev. Microbiol. 15 (2017) 453–464, https://doi.org/10.1038/nrmicro.2017.42.
[15] H.X. Niu, J.Y. Gu, Y. Zhang, Bacterial persisters: molecular mechanisms and therapeutic development, Signal Transduct. Tar. 9 (2024) 174, https://doi.org/10.1038/s41392-024-01866-5.
[16] K. Lewis, The science of antibiotic discovery, Cell 181 (2020) 29–45, https://doi.org/10.1016/j.cell.2020.02.056.
[17] M. Baym, L.K. Stone, R. Kishony, Multidrug evolutionary strategies to reverse antibiotic resistance, Science 351 (2016) aad3292, https://doi.org/10.1126/science.aad3292.
[18] E. Tacconelli, E. Carrara, A. Savoldi, S. Harbarth, M. Mendelson, D.L. Monnet, C. Pulcini, G. Kahlmeter, J. Kluytmans, Y. Carmeli, M. Ouellette, K. Outterson, J. Patel, M. Cavaleri, E.M. Cox, C.R. Houchens, M.L. Grayson, P. Hansen, N. Singh, U. Theuretzbacher, N. Magrini, W.P.P.L. Workin, Discovery, research, and development of new antibiotics: the WHO priority list of antibiotic-resistant bacteria and tuberculosis, Lancet Infect. Dis. 18 (2018) 318–327, https://doi.org/10.1016/S1473-3099(17)30753-3.
[19] B.P. Lazzaro, M. Zasloff, J. Rolff, Antimicrobial peptides: application informed by evolution, Science 368 (2020) eaau5480, https://doi.org/10.1126/science.aau5480.
[20] N.J.r. Oliveira, C.M. Souza, D.F. Buccini, M.H. Cardoso, O.L. Franco, Antimicrobial peptides: structure, functions and translational applications, Nat. Rev. Microbiol. 23 (2025) 687–700, https://doi.org/10.1038/s41579-025-01200-y.
[21] J. Xuan, W. Feng, J. Wang, R. Wang, B. Zhang, L. Bo, Z.-S. Chen, H. Yang, L. Sun, Antimicrobial peptides for combating drug-resistant bacterial infections, Drug Resist. Updat. 68 (2023) 100954, https://doi.org/10.1016/j.drup.2023.100954.
[22] N. Mookherjee, M.A. Anderson, H.P. Haagsman, D.J. Davidson, Antimicrobial host defence peptides: functions and clinical potential, Nat. Rev. Drug Discov. 19 (2020) 311–332, https://doi.org/10.1038/s41573-019-0058-8.
[23] K.A. Brogden, Antimicrobial peptides: pore formers or metabolic inhibitors in bacteria? Nat. Rev. Microbiol. 3 (2005) 238–250, https://doi.org/10.1038/nrmicro1098.
[24] M.A. Cook, G.D. Wright, The past, present, and future of antibiotics, Sci. Transl. Med. 14 (2022) eabo7793, https://doi.org/10.1126/scitranslmed.abo7793.
[25] J.M. Blair, M.A. Webber, A.J. Baylay, D.O. Ogbolu, L.J. Piddock, Molecular mechanisms of antibiotic resistance, Nat. Rev. Microbiol. 13 (2015) 42–51, https://doi.org/10.1038/nrmicro3380.
[26] C.R. Macnair, S.T. Rutherford, M.W. Tan, Alternative therapeutic strategies to treat antibiotic-resistant pathogens, Nat. Rev. Microbiol. 22 (2024) 262–275, https://doi.org/10.1038/s41579-023-00993-0.
[27] M. Mardirossian, R. Grzela, C. Giglione, T. Meinnel, R. Gennaro, P. Mergaert, M. Scocchi, The host antimicrobial peptide Bac71-35 binds to bacterial ribosomal proteins and inhibits protein synthesis, Chem. Biol. 21 (2014) 1639–1647, https://doi.org/10.1016/j.chembiol.2014.10.009.
[28] S. Jekhmane, M.G.N. Derks, S. Maity, C.J. Slingerland, K.H.M.E. Tehrani, J. Medeiros-Silva, V. Charitou, D. Ammerlaan, C. Fetz, N.A. Consoli, R.V. K. Cochrane, E.J. Matheson, M. van der Weijde, B.O.W. Elenbaas, F. Lavore, R. Cox, J.H. Lorent, M. Baldus, M. Künzler, M. Lelli, S.A. Cochrane, N.I. Martin, W.H. Roos,

E. Breukink, M. Weingarth, Host defence peptide plectasin targets bacterial cell wall precursor lipid II by a calcium-sensitive supramolecular mechanism, Nat. Microbiol. 9 (2024) 1778–1791, https://doi.org/10.1038/s41564-024-01696-9.
[29] S.U. Vetterli, K. Zerbe, M. Müller, M. Urfer, M. Mondal, S.Y. Wang, K. Moehle, O. Zerbe, A. Vitale, G. Pessi, L. Eberl, B. Wollscheid, J.A. Robinson, Thanatin targets the intermembrane protein complex required for lipopolysaccharide transport in *Escherichia coli*, Sci. Adv. 4 (2018) eaau2634, https://doi.org/10.1126/sciadv.aau2634.
[30] C.F. Le, C.M. Fang, S.D. Sekaran, Intracellular targeting mechanisms by antimicrobial peptides, Antimicrob. Agents Chemother. 61 (2017) e02340, https://doi.org/10.1128/AAC.02340-16.
[31] Y. Yang, F. Chen, K. Qiao, H. Zhang, H.Y. Chen, K.J. Wang, Two male-specific antimicrobial peptides SCY2 and scyreprocin as crucial molecules participated in the sperm acrosome reaction of mud crab *Scylla paramamosain*, Int. J. Mol. Sci. 23 (2022) 3373, https://doi.org/10.3390/ijms23063373.
[32] Y. Yang, F. Chen, H.Y. Chen, H. Peng, H. Hao, K.J. Wang, A novel antimicrobial peptide scyreprocin from mud crab *Scylla paramamosain* showing potent antifungal and anti-biofilm activity, Front. Microbiol. 11 (2020) 1589, https://doi.org/10.3389/fmicb.2020.01589.
[33] Y. Yang, H.Y. Chen, H. Hao, K.J. Wang, The anticancer activity conferred by the mud crab antimicrobial peptide scyreprocin through apoptosis and membrane disruption, Int. J. Mol. Sci. 23 (2022) 5500, https://doi.org/10.3390/ijms23105500.
[34] Z. Wang, B. Koirala, Y. Hernandez, M. Zimmerman, S.F. Brady, Bioinformatic prospecting and synthesis of a bifunctional lipopeptide antibiotic that evades resistance, Science 376 (2022) 991–996, https://doi.org/10.1126/science.abn4213.
[35] L.M. Ma, Y.R. Wang, M.X. Wang, Y.W. Tian, W. Kang, H.H. Liu, H. Wang, J. Dou, C. L. Zhou, Effective antimicrobial activity of Cbf-14, derived from a cathelin-like domain, against penicillin-resistant bacteria, Biomaterials 87 (2016) 32–45, https://doi.org/10.1016/j.biomaterials.2016.02.011.
[36] Z.Y. Jin, M.L. Shen, L.E. Wang, C. Wang, M.M. Gao, G.Y. Yu, Z.J. Chang, X. W. Zhang, Antibacterial and immunoregulatory activity of an antimicrobial peptide hepcidin in loach (*Misgurnus anguillicaudatus*), Int. J. Biol. Macromol. 242 (2023) 124833, https://doi.org/10.1016/j.ijbiomac.2023.124833.
[37] X. Wang, X. Hong, F. Chen, K.J. Wang, A truncated peptide Spgillcin$_{177\text{-}189}$ derived from mud crab *Scylla paramamosain* exerting multiple antibacterial activities, Front. Cell. Infect. Microbiol. 12 (2022) 928220, https://doi.org/10.3389/fcimb.2022.928220.
[38] J. Mwangi, Y. Yin, G. Wang, M. Yang, Y. Li, Z. Zhang, R. Lai, The antimicrobial peptide ZY4 combats multidrug-resistant *Pseudomonas aeruginosa* and *Acinetobacter baumannii* infection, Proc. Natl. Acad. Sci. U. S. A. 116 (2019) 26516–26522, https://doi.org/10.1073/pnas.1909585117.
[39] J.Y. Xie, M. Zhou, Z.H. Cong, X.M. Xiao, L.Q. Liu, S. Chen, W.A. Jiang, Y.M. Wu, R. H. Liu, A host defense peptide-mimicking prodrug activated by drug-resistant gram-negative bacterial infections, Sci. Transl. Med. 17 (2025) eadl4870, https://doi.org/10.1126/scitranslmed.adl4870.
[40] I. Nicolas, V. Bordeau, A. Bondon, M. Baudy-Floc'h, B. Felden, Novel antibiotics effective against gram-positive and -negative multi-resistant bacteria with limited resistance, PLoS Biol. 17 (2019) e3000337, https://doi.org/10.1371/journal.pbio.3000337.
[41] M.R. Song, Y. Liu, X.Y. Huang, S.Y. Ding, Y. Wang, J.Z. Shen, K. Zhu, A broad-spectrum antibiotic adjuvant reverses multidrug-resistant gram-negative pathogens, Nat. Microbiol. 5 (2020) 1040–1050, https://doi.org/10.1038/s41564-020-0723-z.
[42] H.A. Farrag, N. Abdallah, M.M.K. Shehata, E.M. Awad, Natural outer membrane permeabilizers boost antibiotic action against irradiated resistant bacteria, J. Biomed. Sci. 26 (2019) 69, https://doi.org/10.1186/s12929-019-0561-6.
[43] H. Zhang, Q. Chen, J. Xie, Z. Cong, C. Cao, W. Zhang, D. Zhang, S. Chen, J. Gu, S. Deng, Z. Qiao, X. Zhang, M. Li, Z. Lu, R. Liu, Switching from membrane disrupting to membrane crossing, an effective strategy in designing antibacterial polypeptide, Sci. Adv. 9 (2023) eabn0771, https://doi.org/10.1126/sciadv.abn0771.
[44] D. Nagarajan, N. Roy, O. Kulkarni, N. Nanajkar, A. Datey, S. Ravichandran, C. Thakur, S. T, I.V. Aprameya, S.P. Sarma, D. Chakravortty, N. Chandra, Ω76: a designed antimicrobial peptide to combat carbapenem- and tigecycline-resistant *Acinetobacter baumannii*, Sci. Adv. 5 (2019) eaax1946, https://doi.org/10.1126/sciadv.aax1946.
[45] Y.B. Lin, M.A. Sanson, L.A. Vega, B. Shah, S. Regmi, M.B. Cubria, A.R. Flores, ExPortal and the LiaFSR regulatory system coordinate the response to cell membrane stress in *Streptococcus pyogenes*, Mbio 11 (2020) e01804–e01820, https://doi.org/10.1128/mBio.01804-20.
[46] A. de Breij, M. Riool, R.A. Cordfunke, N. Malanovic, L. de Boer, R.I. Koning, E. Ravensbergen, M. Franken, T. van der Heijde, B.K. Boekema, P.H.S. Kwakman, N. Kamp, A. El Ghalbzouri, K. Lohner, S.A.J. Zaat, J.W. Drijfhout, P.H. Nibbering, The antimicrobial peptide SAAP-148 combats drug-resistant bacteria and biofilms, Sci. Transl. Med. 10 (2018) eaan4044, https://doi.org/10.1126/scitranslmed.aan4044.
[47] J.R. Shi, C. Chen, D.J. Wang, Z.Q. Wang, Y. Liu, The antimicrobial peptide LI14 combats multidrug-resistant bacterial infections, Commun. Biol. 5 (2022) 926, https://doi.org/10.1038/s42003-022-03899-4.
[48] S.L. Bai, J.X. Wang, K.L. Yang, C.L. Zhou, Y.F. Xu, J.F. Song, Y.X. Gu, Z. Chen, M. Wang, C. Shoen, B. Andrade, M. Cynamon, K. Zhou, H. Wang, Q.Y. Cai, E. Oldfield, S.C. Zimmerman, Y.G. Bai, X.X. Feng, A polymeric approach toward resistance-resistant antimicrobial agent with dual-selective mechanisms of action, Sci. Adv. 7 (2021) eabc9917, https://doi.org/10.1126/sciadv.abc9917.
[49] T.F. Durand-Reville, A.A. Miller, J.P. O'Donnell, X.Y. Wu, M.A. Sylvester, S. Guler, R. Iyer, A.B. Shapiro, N.M. Carter, C. Velez-Vega, S.H. Moussa, S.M. McLeod, A. Chen, A.M. Tanudra, J. Zhang, J. Comita-Prevoir, J.A. Romero, H. Huynh, A. D. Ferguson, P.S. Horanyi, S.J. Mayclin, H.S. Heine, G.L. Drusano, J.E. Cummings, R.A. Slayden, R.A. Tommasi, Rational design of a new antibiotic class for drug-resistant infections, Nature 597 (2021) 698, https://doi.org/10.1038/s41586-021-03899-0.
[50] J. Lakshmaiah Narayana, B. Mishra, T. Lushnikova, Q. Wu, Y.S. Chhonker, Y. Zhang, D. Zarena, E.S. Salnikov, X. Dang, F. Wang, C. Murphy, K.W. Foster, S. Gorantla, B. Bechinger, D.J. Murry, G. Wang, Two distinct amphipathic peptide antibiotics with systemic efficacy, Proc. Natl. Acad. Sci. U. S. A. 117 (2020) 19446–19454, https://doi.org/10.1073/pnas.2005540117.
[51] H. Van Acker, T. Coenye, The role of reactive oxygen species in antibiotic-mediated killing of bacteria, Trends Microbiol. 25 (2017) 456–466, https://doi.org/10.1016/j.tim.2016.12.008.
[52] Clinical and Laboratory Standards Institute, Performance Standards for Antimicrobial Susceptibility Testing. https://clsi.org/shop/standards/m100/, 2023 (accessed 22 March 2026).
[53] European Committee on Antimicrobial Susceptibility Testing, Clinical Breakpoints and Dosing of Antibiotics. https://www.eucast.org/clinical_breakpoints_and_dosing/eucast_setting_breakpoints/, 2024 (accessed 23 March 2026).
[54] V. Choi, J.L. Rohn, P. Stoodley, D. Carugo, E. Stride, Drug delivery strategies for antibiofilm therapy, Nat. Rev. Microbiol. 21 (2023) 555–572, https://doi.org/10.1038/s41579-023-00905-2.
[55] E.J. Filippone, W.K. Kraft, J.L. Farber, The nephrotoxicity of vancomycin, Clin. Pharmacol. Ther. 102 (2017) 459–469, https://doi.org/10.1002/cpt.726.
[56] A. Ordooei Javan, S. Shokouhi, Z. Sahraei, A review on colistin nephrotoxicity, Eur. J. Clin. Pharmacol. 71 (2015) 801–810, https://doi.org/10.1007/s00228-015-1865-4.
[57] H. Raghuraman, A. Chattopadhyay, Melittin: a membrane-active peptide with diverse functions, Biosci. Rep. 27 (2007) 189–223, https://doi.org/10.1007/s10540-006-9030-z.
[58] R. Laxminarayan, D. Sridhar, M. Blaser, M. Wang, M. Woolhouse, Achieving global targets for antimicrobial resistance, Science 353 (2016) 874–875, https://doi.org/10.1126/science.aaf9286.
[59] A.H. Holmes, L.S. Moore, A. Sundsfjord, M. Steinbakk, S. Regmi, A. Karkey, P. J. Guerin, L.J. Piddock, Understanding the mechanisms and drivers of antimicrobial resistance, Lancet 387 (2016) 176–187, https://doi.org/10.1016/S0140-6736(15)00473-0.
[60] E.M. Darby, E. Trampari, P. Siasat, M.S. Gaya, I. Alav, M.A. Webber, J.M.A. Blair, Molecular mechanisms of antibiotic resistance revisited, Nat. Rev. Microbiol. 21 (2023) 280–295, https://doi.org/10.1038/s41579-022-00820-y.
[61] S. Saha, R. Kar, K. Sikder, D. Manna, R.R. Pal, S. Chakraborti, A.H. Khan, S. Barman, A.R. Maity, A. Basu, Deciphering the inhibitory mechanism of antimicrobial peptide pexiganan conjugated with sodium-alginate chitosan-cholesterol nanoparticle against the opportunistic pathogen, J. Drug Delivery Sci. Technol. 101 (2024) 106305, https://doi.org/10.1016/j.jddst.2024.106305.
[62] X.J. Wang, X.L. Xu, S.J. Zhang, N. Chen, Y.F. Sun, K.F. Ma, D.S. Hong, L. Li, Y. Z. Du, X.Y. Lu, S.P. Jiang, TPGS-based and S-thanatin functionalized nanorods for overcoming drug resistance in *Klebsiella pneumonia*, Nat. Commun. 13 (2022) 3731, https://doi.org/10.1038/s41467-022-31500-3.
[63] M.D.T. Torres, E.F. Brooks, A. Cesaro, H. Sberro, M.O. Gill, C. Nicolaou, A.S. Bhatt, C. de la Fuente-nunez, Mining human microbiomes reveals an untapped source of peptide antibiotics, Cell 187 (2024) 5453–5467, https://doi.org/10.1016/j.cell.2024.07.027.
[64] J. Qiu, D. Wu, C. Xu, Y. Zhuang, Y. Lu, A. sun, X. Lu, J. Han, L. Ni, Current advances and emerging prospects of specifically targeted antimicrobial peptides: a comprehensive review, Int. J. Biol. Macromol. 322 (2025) 147037, https://doi.org/10.1016/j.ijbiomac.2025.147037.
[65] H. Koo, R.N. Allan, R.P. Howlin, P. Stoodley, L. Hall-Stoodley, Targeting microbial biofilms: current and prospective therapeutic strategies, Nat. Rev. Microbiol. 15 (2017) 740–755, https://doi.org/10.1038/nrmicro.2017.99.
[66] K. Gerdes, S. Semsey, Microbiology: pumping persisters, Nature 534 (2016) 41–42, https://doi.org/10.1038/nature18442.
[67] A. Boaro, L. Ageitos, M.D.T. Torres, E.B. Blasco, S. Oztekin, C. de la Fuente-nunez, Structure-function-guided design of synthetic peptides with anti-infective activity derived from wasp venom, Cell Rep. Phys. Sci. 4 (2023) 101459, https://doi.org/10.1016/j.xcrp.2023.101459.
[68] Y.B. Liang, Y.H. Zhang, Y. Huang, C. Xu, J.X. Chen, X.S. Zhang, B.C. Huang, Z. H. Gan, X.H. Dong, S.Y. Huang, C.R. Li, S.Y. Jia, P.F. Zhang, Y.L. Yuan, H.B. Zhang, Y.C. Wang, B. Yuan, Y. Bao, S.Y. Xiao, M.H. Xiong, Helicity-directed recognition of bacterial phospholipid via radially amphiphilic antimicrobial peptides, Sci. Adv. 10 (2024) eadn9435, https://doi.org/10.1126/sciadv.adn9435.
[69] W. Kim, G.J. Zou, T.P.A. Hari, I.K. Wilt, W.P. Zhu, N. Galle, H.A. Faizi, G. L. Hendricks, K. Tori, W. Pan, X.W. Huang, A.D. Steele, E.E. Csatary, M. M. Dekarske, J.L. Rosen, N.D. Ribeiro, K. Lee, J. Port, B.B. Fuchs, P.M. Vlahovska, W.M. Wuest, H.J. Gao, F.M. Ausubel, E. Mylonakis, A selective membrane-targeting repurposed antibiotic with activity against persistent methicillin-resistant *Staphylococcus aureus*, P. Natl. Acad. Sci. U. S. A. 116 (2019) 16529–16534, https://doi.org/10.1073/pnas.1904700116.
[70] D. Saeloh, V. Tipmanee, K.K. Jim, M.P. Dekker, W. Bitter, S.P. Voravuthikunchai, M. Wenzel, L.W. Hamoen, The novel antibiotic rhodomyrtone traps membrane proteins in vesicles with increased fluidity, PLoS Pathog. 14 (2018) e1006876, https://doi.org/10.1371/journal.ppat.1006876.

[71] C. Huang, H. Jin, Y. Qian, S. Qi, H. Luo, Q. Luo, Z. Zhang, Hybrid melittin cytolytic peptide-driven ultrasmall lipid nanoparticles block melanoma growth *in vivo*, ACS Nano 7 (2013) 5791–5800, https://doi.org/10.1021/nn400683s.
[72] A. Loewa, J.J. Feng, S. Hedtrich, Human disease models in drug development, Nat. Rev. Bioeng. 1 (2023) 545–559, https://doi.org/10.1038/s44222-023-00063-3.
[73] R.A.G. da Silva, J.J. Wong, H. Antypas, P.Y. Choo, K. Goh, S. Jolly, C. Liang, L.T. K. Sing, M. Veleba, G.A. Hu, J.Z. Chen, K.A. Kline, Mitoxantrone targets both host and bacteria to overcome vancomycin resistance in *Enterococcus faecalis*, Sci. Adv. 9 (2023) eadd9280, https://doi.org/10.1126/sciadv.add9280.
[74] B.A. Lipsky, K.J. Holroyd, M. Zasloff, Topical versus systemic antimicrobial therapy for treating mildly infected diabetic foot ulcers: a randomized, controlled, double-blinded, multicenter trial of pexiganan cream, Clin. Infect. Dis. 47 (2008) 1537–1545, https://doi.org/10.1086/593185.
[75] J.A. Bengoechea, J. Sa Pessoa, *Klebsiella pneumoniae* infection biology: living to counteract host defences, FEMS Microbiol. Rev. 43 (2019) 123–144, https://doi.org/10.1093/femsre/fuy043.